NC STATE UNIVERSITY

Geotechnical Engineering at the Grain Scale

T. Matthew Evans

Department of Civil, Construction, and Environmental Engineering

North Carolina State University

Graduate Students: Bahador, Cunningham, Kress, Ning, Wang, Zhao

Collaborators: Chall (RENCI), Gabr (NCSU), Rhyne (RENCI), Tayebali (NCSU), Frost (GT), Valdes (SDSU), Yun (Yonsei), Andrade (Caltech)

Funding: NSF, NASA, FHWA, NCDOT

Preliminaries

NCSU: Geotechnical Engineering

- 5 Full-time faculty (one starting January 2012)
- Excellent breadth in research interests, from the very small (particle-level) scale to full field scale, from highly theoretical to very applied, experimental and numerical
- 13 full-time graduate students (11 supported) and a comparable number of part-time students

- Wide variety of courses offered:
  - Advanced Soil Mechanics (2 courses)
  - Unsaturated Soil Mechanics
  - Geosynthetics
  - Foundation Design
  - Laboratory Methods
  - Soil Dynamics
  - Numerical Methods
  - Groundwater Hydrology
  - Rock Mechanics
  - Special Topics Courses

Preliminaries

NCSU: Geotechnical Engineering

The Effects of Loading Conditions on Material Response: Discrete Numerical Studies

- Simulations of multiple laboratory tests
- Quantification and analysis of microstructure evolution
- Why does material response vary with boundary conditions?
- Are common laboratory parameters sufficient for design?
- Why or why not?

Geotechnical systems are often subjected to plane strain loading, but designs are based on axisymmetric testing.

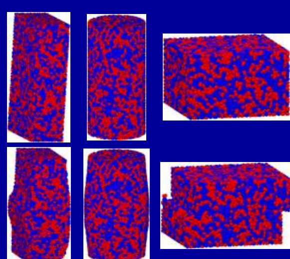

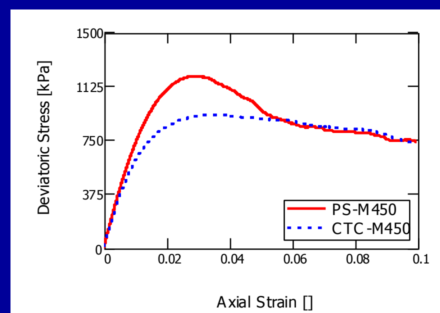

Sponsor: NCSU Department of Civil, Construction, and Environmental Engineering and the NCSU College of Engineering

Preliminaries

NCSU: Geotechnical Engineering

Visualization of Three-Dimensional Discrete Numerical Data

- The microstructure of granular materials governs the design-scale behavior
- Laboratory investigation of microstructure is expensive, time-consuming, and requires highly specialized equipment
- Numerical studies are faster and less expensive, yet it has not previously been possible to directly compare experimental and numerical results
- Current research will allow for equivalent measurements to be made on physical and numerical specimens

The microstructure of particulate systems can be studied experimentally or numerically, but it is often not possible to compare results from the two methods.

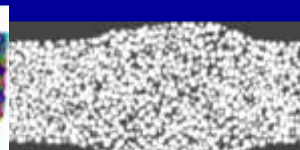

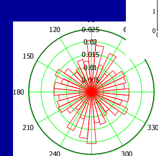

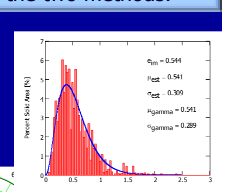

Collaborators: Theresa-Marie Rhyne and Steve Chall, Renaissance Computing Institute (RENCI@NCSU)
Sponsors: NCSU Department of CCEE, NCSU COE, North Carolina General Assembly

NCSU: Geotechnical Engineering

The Effects of Grain Size Distribution Aggregate Base Course Performance

- Rejecting material at the job site (or quarry) results in unnecessary expense and delays
- Prepare specimens at varying GSD's
- Assess GSD impacts on material response
- Use numerical tools to investigate underlying mechanisms
- Can "out-of-spec" material be safely used in some projects?

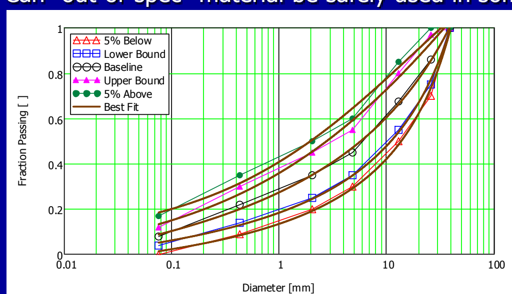

The current NCDOT requirement for ABC material is an *ad-hoc* specification based solely on the grain size distribution.

Sponsor: North Carolina Department of Transportation (NCDOT)

NCSU: Geotechnical Engineering

Field-Scale Research, Including Reinforced Earth, Pile Bents, and Undercut in Construction

Preliminaries

NCSU: Geotechnical Engineering

Field-Scale Research, Including Reinforced Earth, Pile Bents, and Undercut in Construction

Preliminaries

NCSU: Geotechnical Engineering

Remote Monitoring of Geostructural Health

- Two earth dams and a large load frame on the NCSU Centennial Campus have been instrumented for monitoring
- Pore water pressures, dam movement, and strains in the steel superstructure are monitored
- Data are transmitted wirelessly and automatically databased and posted to the project website
- Visit http://www.ce.ncsu.edu/ccli-sensors

Post-construction monitoring of large geostructures is increasingly frequent. We study the best approaches to monitoring and teach students to use these technologies in their careers.

Sponsors: U.S. National Science Foundation

Geotech Faculty at NCSU

- Dr. Roy Borden
  - Classical and applied geotechnics
  - Shallow and deep foundations
  - Reinforced soil and earth walls
  - Soil-structure interaction

Preliminaries

Geotech Faculty at NCSU

- Dr. Mo Gabr
  - Geoenvironmental engineering
  - Geosynthetics
  - Deep foundations
  - Transportation geotechnics

Geotech Faculty at NCSU

- Brina Mortensen
  - Bio-mediated soil improvement
  - Identification and behavior of naturally cemented and aged sands
  - Sustainable building materials

Geotech Faculty at NCSU

- Dr. Shamim Rahman
  - Modeling and computing in geomechanics
  - Soil dynamics
  - Seabed mechanics
  - Stochastic and neuro-fuzzy modeling

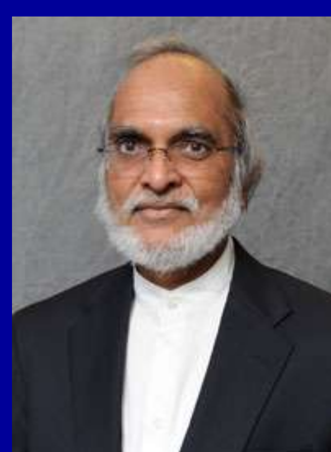

Geotech Faculty at NCSU

- Dr. Matt Evans
  - Granular mechanics and particulate behavior
  - Energy geotechnics
  - Extraterrestrial geomechanics
  - Multiphysics processes
  - Unsaturated soil mechanics
  - Image analysis and microstructure quantification

Motivation

- Soils are a fundamentally discrete, rather than a continuum, material
- To capture the inherent nonlinearity, heterogeneity, and anisotropy in soils, their granular nature must be considered
- Many engineering-scale behaviors can be explained (or at least inferred) by considering response at the granular level

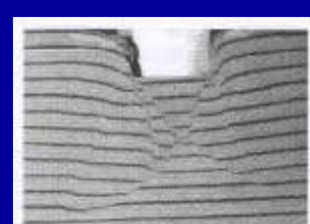

From Tatsuoka, 2002

From Nübel, 2002

Motivation (cont.)

- Interfaces, grain crushing, bonded and unbonded material, and strain softening cannot be readily captured in continuum models
- We can use the discrete element method (DEM) simulations to quantify granular response across a range of spatial and temporal scales

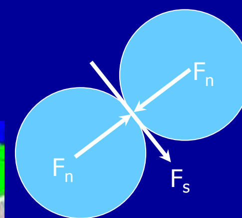

Overview

- Soil micromechanics
- Discrete element method (DEM)
- Integrated Numerical-Experimental Study
- DEM Simulations: Effects of Geometry
- Soil-Structure Interaction (SSI)
- Thermal Conductivity
- Summary and Conclusions

Soil Micromechanics

Hertzian Contacts

$$\delta = \frac{1}{2\cdot R^{\frac{1}{3}}}\cdot\left[\frac{3\cdot\left(1-\nu_g\right)}{G_g}\cdot N\right]^{\frac{2}{3}}$$

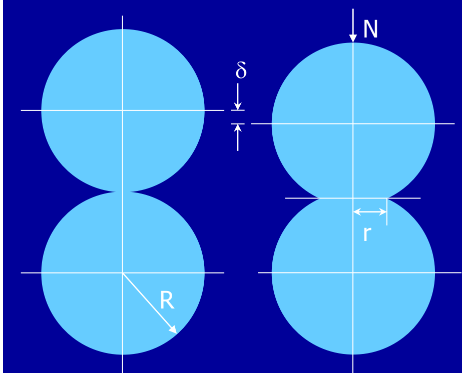

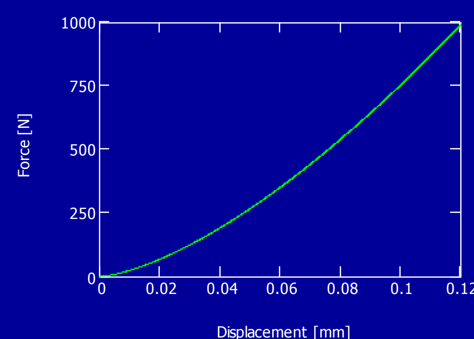

(after Santamarina, et al., 2001)

Soil Micromechanics

Tangential Loading: Hertz-Mindlin

Displacement at yield:

$$\delta_y = \frac{3}{8}\cdot\left(2-\nu_g\right)\cdot\frac{\mu\cdot N}{G_g\cdot\left[R\cdot\sqrt[3]{\frac{3\cdot\left(1-\nu_g\right)\cdot N}{8\cdot G_g\cdot R^2}}\right]}$$

Tangential displacement:

$$\delta_{tan} = \left[1-\left(1-\frac{T}{\mu\cdot N}\right)^{\frac{2}{3}}\right]\cdot\delta_y$$

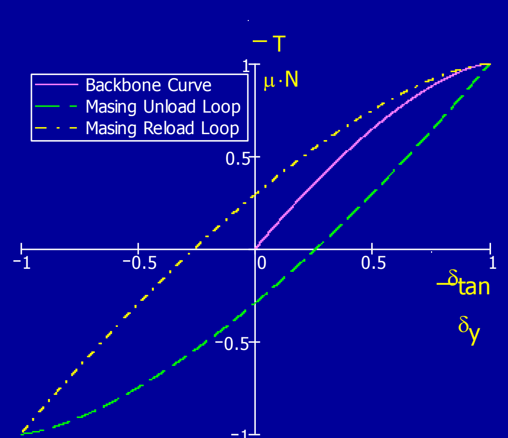

(after Santamarina, et al., 2001)

Soil Micromechanics

Fabric Failure

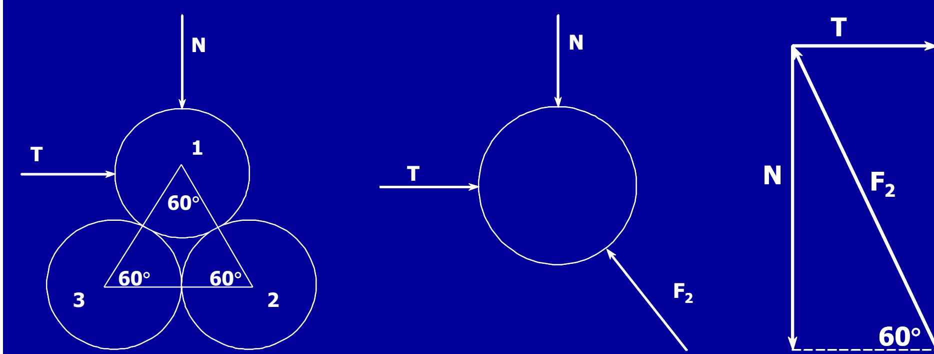

Force required to cause fabric failure: $T_f = N \cdot \tan(30)$

Soil Micromechanics

Shear Strain to Failure

From geometry: $$\gamma_f = \frac{\Delta r_{12} \cdot \left(1 - \frac{\Delta r_{12}}{4 \cdot R}\right)}{2 \cdot R \cdot \cos(30\mathrm{deg})}$$

Force as a function of confining stress: $$N = 4 \cdot R^2 \cdot \sigma_c$$

Material properties for quartz grains:

$G_g = 29 \cdot \mathrm{GPa}$ $\nu_g = 0.25$ $\mu_g = 0.5$

Threshold failure strains:

$$\gamma_{fabric} = 1.4 \cdot 10^{-5} \left(\frac{\sigma}{\mathrm{kPa}}\right)^{\frac{2}{3}}$$

$$\gamma_{slip} = 6.7 \cdot 10^{-6} \left(\frac{\sigma}{\mathrm{kPa}}\right)^{\frac{2}{3}}$$

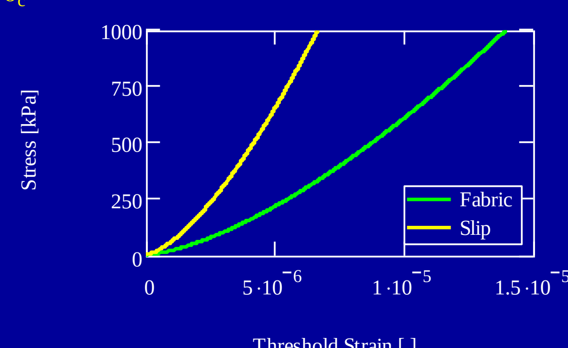

(after Santamarina, et al., 2001)

Rotational Frustration

- Dilation in dense granular systems

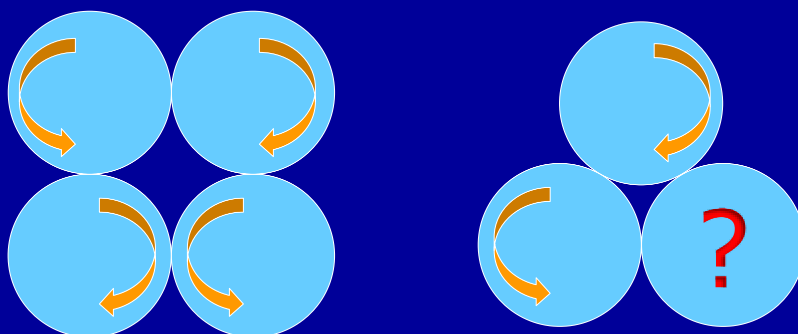

Even very simple models can be used to indicate the propensity for rotational frustration in a dense granular system. Energy must be dissipated through contact dissolution and formation if particles are unable to rotate even at very small strains.

Lateral Earth Stress at Rest

- ($K_0 = P_x/P_y$)

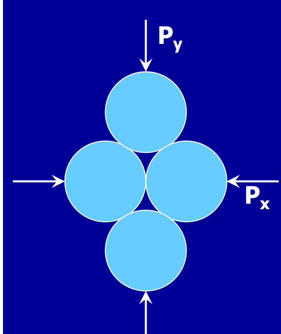

From a force balance: $K_0 = \tan(30) = 0.577$

From continuum mechanics ($\nu = 0.3$): $K_0 = \dfrac{\nu}{1-\nu} = 0.429$

Jaky, 1944 ($\phi' = 30°$):

$$K_0 = (1-\sin(\phi))\cdot\frac{1+\frac{2}{3}\sin(\phi)}{1+\sin(\phi)} = 0.444$$

Jaky, 1948 ($\phi' = 30°$): $K_0 = 1 - \sin(30) = 0.5$

Note that for $\phi' = 25°$ and $\nu = 0.366$, the geometric, continuum, and Jaky (1948) solutions are equivalent (i.e., $K_0 = 0.577$).

Filter Criteria: Grain Size Distribution

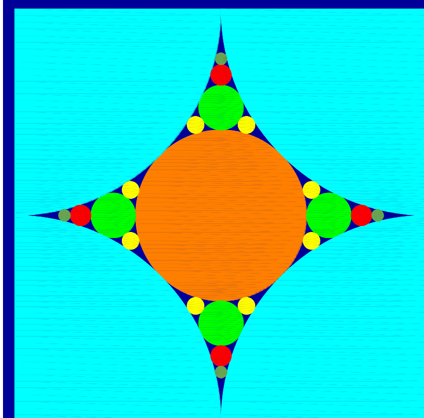

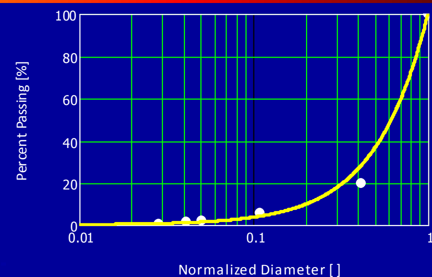

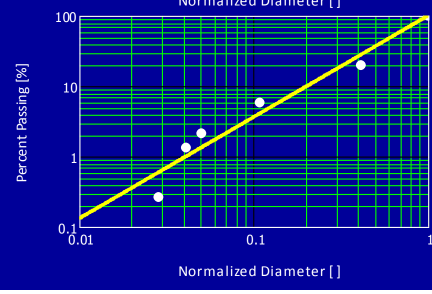

Talbot relationship: $P_p = 100 \cdot \left(\frac{d}{d_{max}} \right)^{\beta}$

Unsaturated Soils

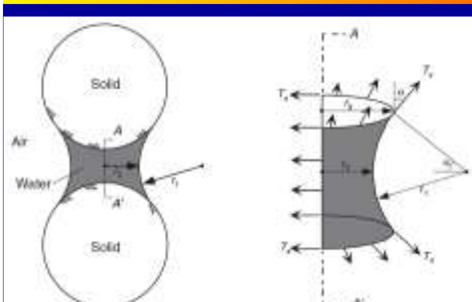

The force acting between the two particles is:

$$F = \Delta u \cdot \pi \cdot r_2^2 + T_s \cdot 2 \cdot \pi \cdot r_2$$

We can get Δu from the Young-Laplace equatic

$$\Delta u = T_s \cdot \left(\frac{1}{r_1} + \frac{1}{r_2} \right)$$

A simple geometric argument tells us that:

$$\left(R + r_1\right)^2 = R^2 + \left(r_1 + r_2\right)^2$$

Solving for r_1 we can express Young-Laplace in terms of r_2 and R only:

$$r_1 = \frac{1}{2} \cdot \frac{r_2^2}{R - r_2} \qquad \Delta u = T_s \cdot \left(\frac{1}{\frac{1}{2} \cdot \frac{r_2^2}{R - r_2}} - \frac{1}{r_2} \right)$$

Note that r_1 and r_2 must have different signs in the Young-Laplace equation because they contribute to opposite pressures. Simplifying the expression for Δu gives:

$$\Delta u = T_s \cdot \frac{2 \cdot R - 3 \cdot r_2}{r_2^2}$$

(after Santamarina, et al., 2001; Lu and Likos, 2004)

Soil Micromechanics

Unsaturated Soils

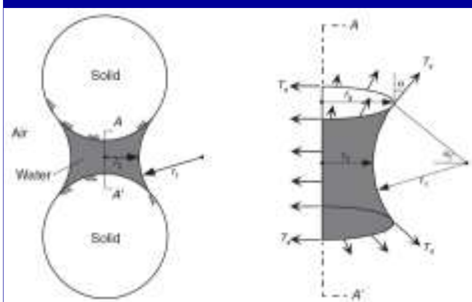

Thus, the expression for the force between the two particles due to capillarity may be expressed as:

$$F = T_s \cdot \frac{2 \cdot R - 3 \cdot r_2}{r_2^2} \cdot \pi \cdot r_2^2 + T_s \cdot 2 \cdot \pi \cdot r_2$$

Or, simplifying: $F = (2 \cdot R - r_2) \cdot T_s \cdot \pi$

Normalizing by an area of $(2R)^2$ provides an expression for the equivalent effective stress due to capillarity:

$$\sigma' = \frac{F}{(2 \cdot R)^2} \qquad \sigma' = \frac{T_s \cdot \pi}{4 \cdot R^2} \cdot (2 \cdot R - r_2)$$

From the above argument it is possible to calculate effective stress without measuring matric suction. This is significant because matric suction is such an elusive quantity to measure.

Using a similar approach, effective stress between to face-to-face platy particles may be calculated as:

$$\sigma' = \frac{\pi}{4} \cdot T_s \cdot \left(\frac{S_a \cdot \gamma_w}{w \cdot g} \right)$$ where S_a is specific surface area.

(after Santamarina, et al., 2001; Lu and Likos, 2004)

Soil Micromechanics

Unsaturated Soils

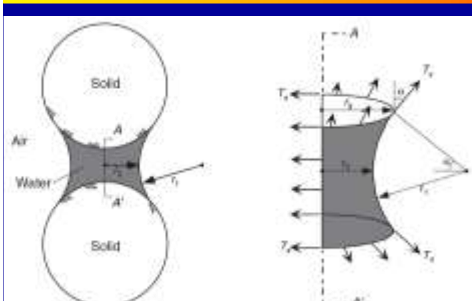

Now let's calculate the water content of our system. The half-height of the meniscus can be expressed as:

$$R^2 = r_2^2 + (R - h)^2 \qquad h = R - \sqrt{R^2 - r_2^2}$$

If we assume that the meniscus is a cylinder of height 2h and radius r_2, we can calculate its volume:

$$V_w = \pi \cdot r_2^2 \cdot (2 \cdot h) - 2 \cdot \frac{1}{3} \cdot \pi \cdot h^2 \cdot (3 \cdot R - h)$$

Noting that the coordination number (cn) for a simple cubic (SC) packing is 6, each particle will be associated with six half-menisci. Water content is then calculated as:

$$w = \frac{6 \cdot \frac{V_w}{2} \cdot \rho_w}{\frac{4}{3} \cdot \pi \cdot R^3 \cdot \rho_s} \qquad w = \frac{9}{4} \cdot \frac{V_w}{\pi \cdot R^3 \cdot G_s}$$

After a bit of algebraic acrobatics, we get the follow

$$w = \frac{9}{8} \cdot \frac{\lambda^4}{G_s} \qquad \text{where:} \qquad \lambda = \frac{r_2}{R}$$

This calculation of water content (an easily measurable quantity) is significant because it allows us to remove r_2 (which isn't easy to measure) from our subsequent equations.

(after Santamarina, et al., 2001; Lu and Likos, 2004)

Soil Micromechanics

Unsaturated Soils

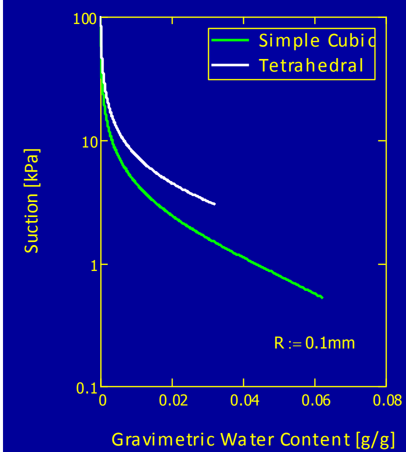

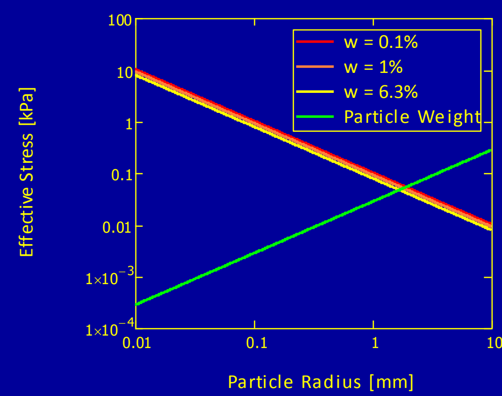

Preliminaries

Overview

- Soil micromechanics
- Discrete element method (DEM)
- Integrated Numerical-Experimental Study
- DEM Simulations: Effects of Geometry
- Soil-Structure Interaction (SSI)
- Thermal Conductivity
- Summary and Conclusions

Discrete Element Method

DEM: Introduction

- Increasingly popular in research
  - Used to gain insight into particulate behavior
  - Calibrated to simulate macroscale laboratory results
  - Microstructure output consists of quantities not readily measurable in real soils
  - Microstructure can also be quantified using many of the same approaches used for physical experiments
- Not yet widely used in practice
  - Inertia / skepticism / unfamiliarity

Discrete Element Method

Model Fundamentals

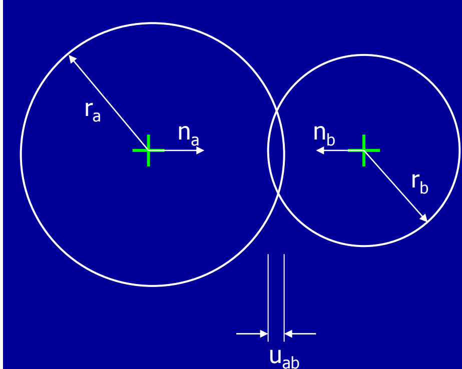

Solution of Newton's EOM for each particle:

- Calculate contact normals
- Determine overlap and contact locations
- Calculate relative positions and velocities
- Use constitutive relations
- Calculate new forces/moments

Model Assemblies: Particle Shape

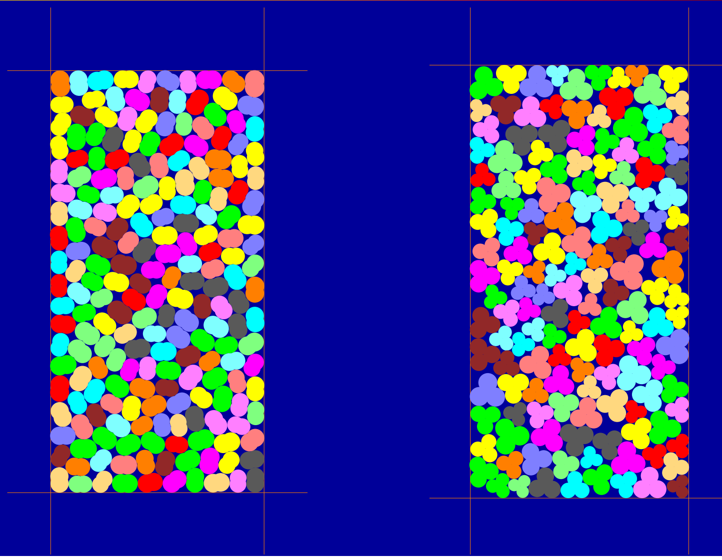

Discrete Element Method

Model Assemblies: Specimen Geometry

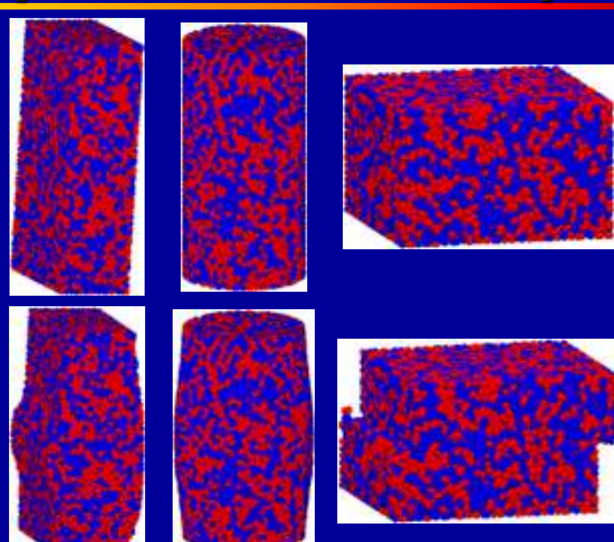

Microstructural Parameters

Displacement Vectors

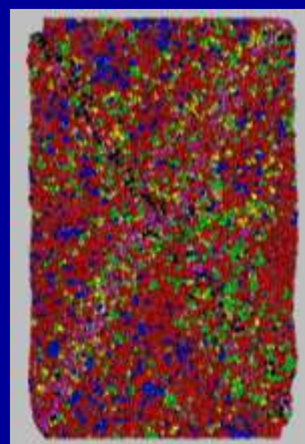

Particle Rotations

Normal Contact Forces

Bridging Scales: the Stress-Force-Fabric Relationship

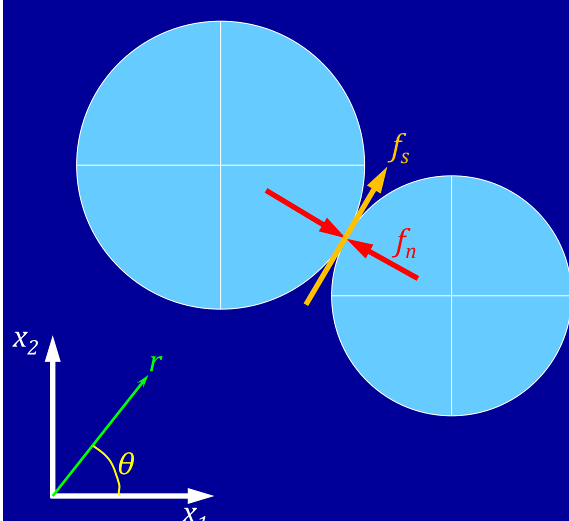

At any contact in the assembly, the mechanics can be defined by the magnitude and orientation of the contact normal and shear force vectors.

By assembling this information for every contact in the assembly, we can know something about the stresses at the specimen scale.

Discrete Element Method

Bridging Scales: the Stress-Force-Fabric Relationship

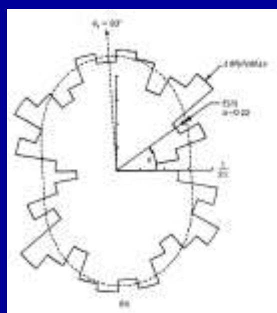

Contact Orientation

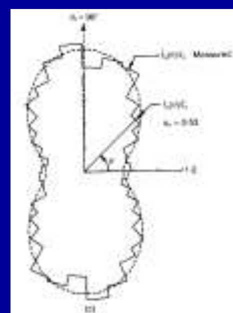

Normal Force

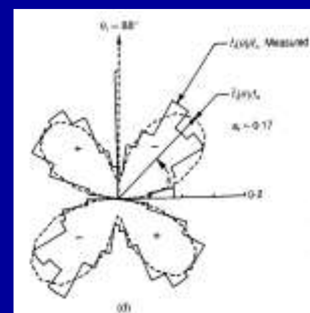

Tangential Force

$$E(\theta) = \frac{1}{2\cdot\pi}\cdot\left[1 + a_c\cdot\cos\left[2\cdot\left(\theta - \theta_a\right)\right]\right]$$

$$N(\theta) = -N_0\cdot\left[1 + a_n\cdot\cos\left[2\cdot\left(\theta - \theta_f\right)\right]\right]$$

$$T(\theta) = -N_0\cdot\left[a_t\cdot\sin\left[2\cdot\left(\theta - \theta_f\right)\right]\right]$$

Note the fitting parameters to the Fourier expansions above: a_c, a_n, and a_t.

(Rothenburg and Bathurst, 1992)

Discrete Element Method

Stress-Force-Fabric Relationship

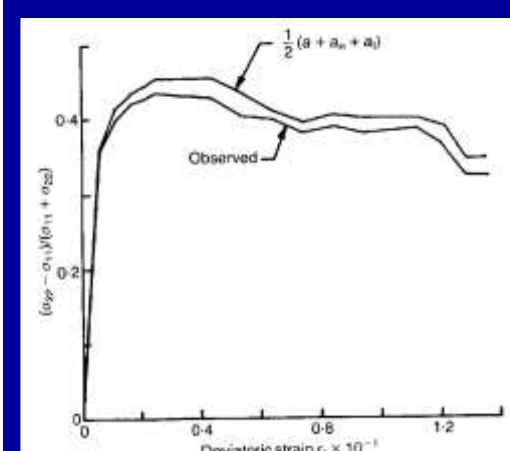

The theoretical stress-force-fabric relationship derived from fabric tensors and microscale stress quantities:

$$\sin\left(\frac{\sigma_{11} - \sigma_{22}}{\sigma_{11} + \sigma_{22}}\right) = \frac{1}{2}\cdot\left(a_c + a_n + a_t\right)$$

(Rothenburg and Bathurst, 1992)

Simulation of Real Systems and Processes

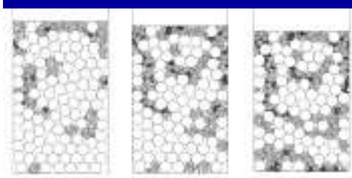

Particle Crushing (Lobo-Guerrero, 2006)

Direct Shear Test (Liu, 2006)

Cone Penetration
(Jiang, et al., 2006)

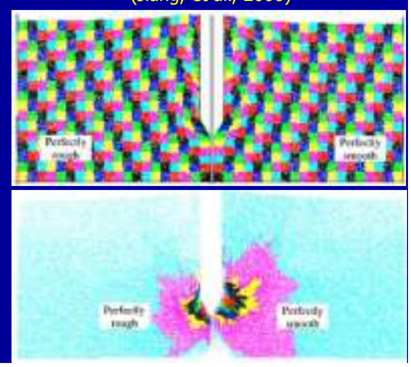

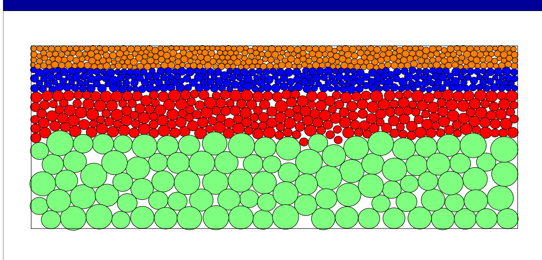

Layered Systems (e.g., pavements)

Overview

- Soil micromechanics
- Discrete element method (DEM)
- Integrated Numerical-Experimental Study
- DEM Simulations: Effects of Geometry
- Soil-Structure Interaction (SSI)
- Thermal Conductivity
- Summary and Conclusions

Integrated N-E Study

Plane Strain Testing

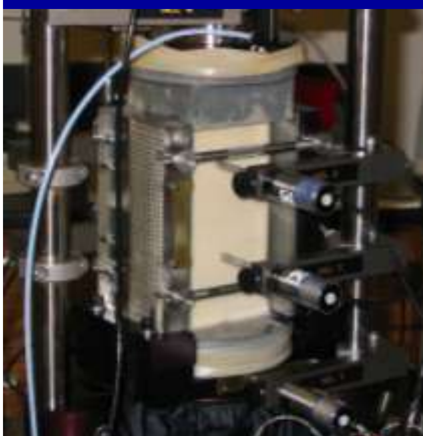

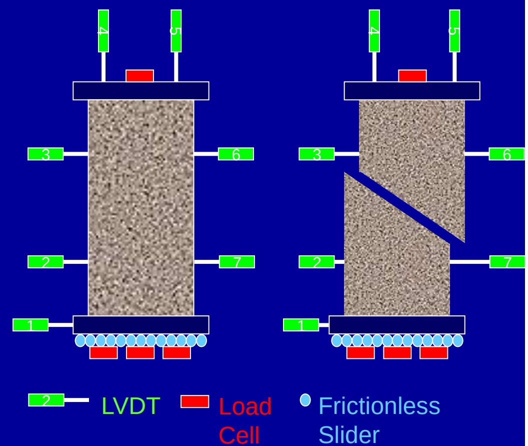

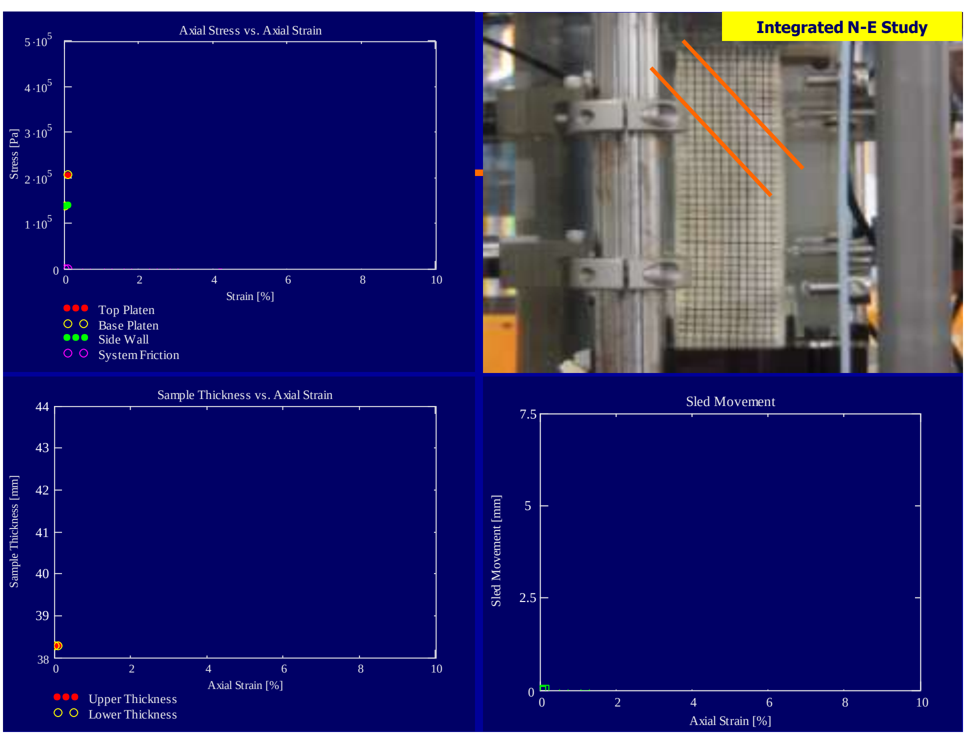

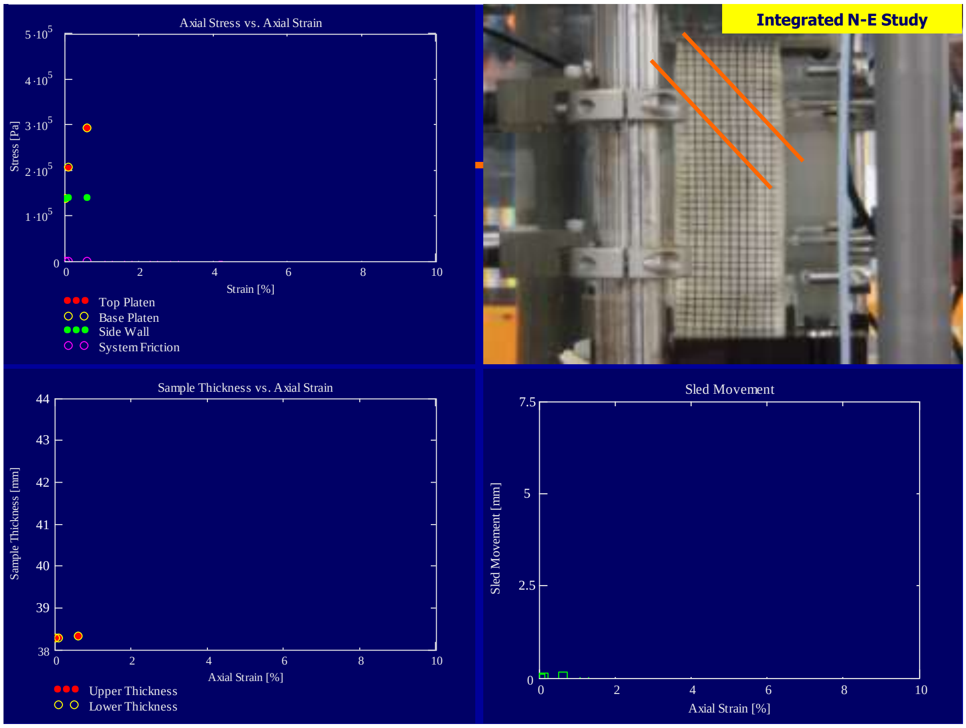
Axial Stress vs. Axial Strain
Stress [Pa]
Strain [%]
Top Platen
Base Platen
Side Wall
System Friction
Integrated N-E Study
Sample Thickness vs. Axial Strain
Sample Thickness [mm]
Axial Strain [%]
Upper Thickness
Lower Thickness
Sled Movement
Sled Movement [mm]
Axial Strain [%]

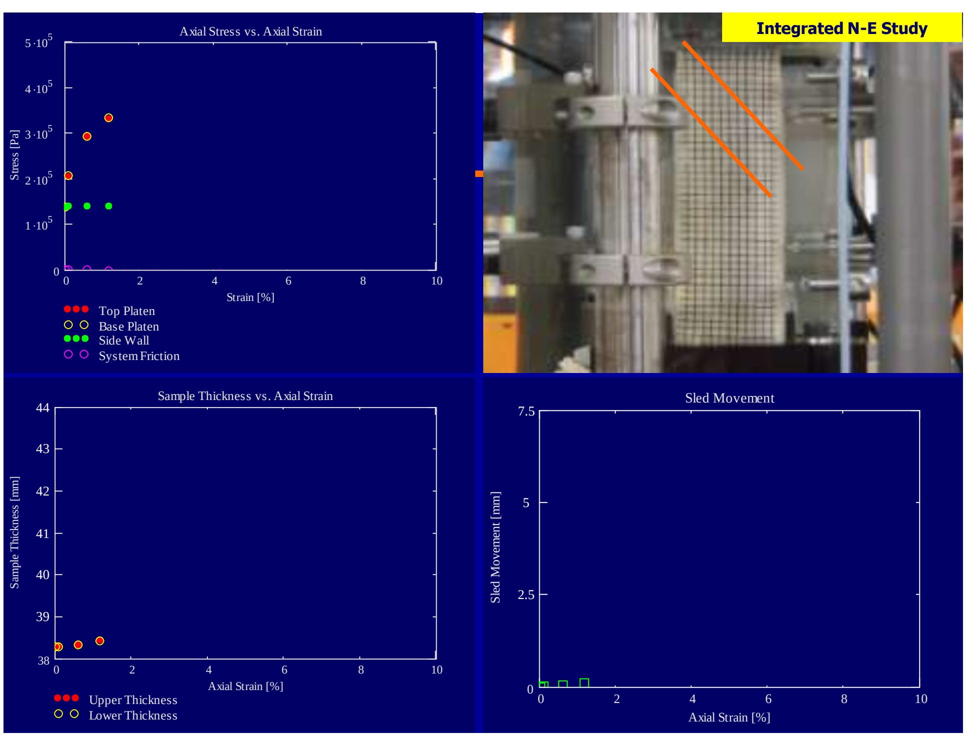
Axial Stress vs. Axial Strain
Stress [Pa]
Strain [%]
Top Platen
Base Platen
Side Wall
System Friction
Integrated N-E Study
Sample Thickness vs. Axial Strain
Sample Thickness [mm]
Axial Strain [%]
Upper Thickness
Lower Thickness
Sled Movement
Sled Movement [mm]
Axial Strain [%]

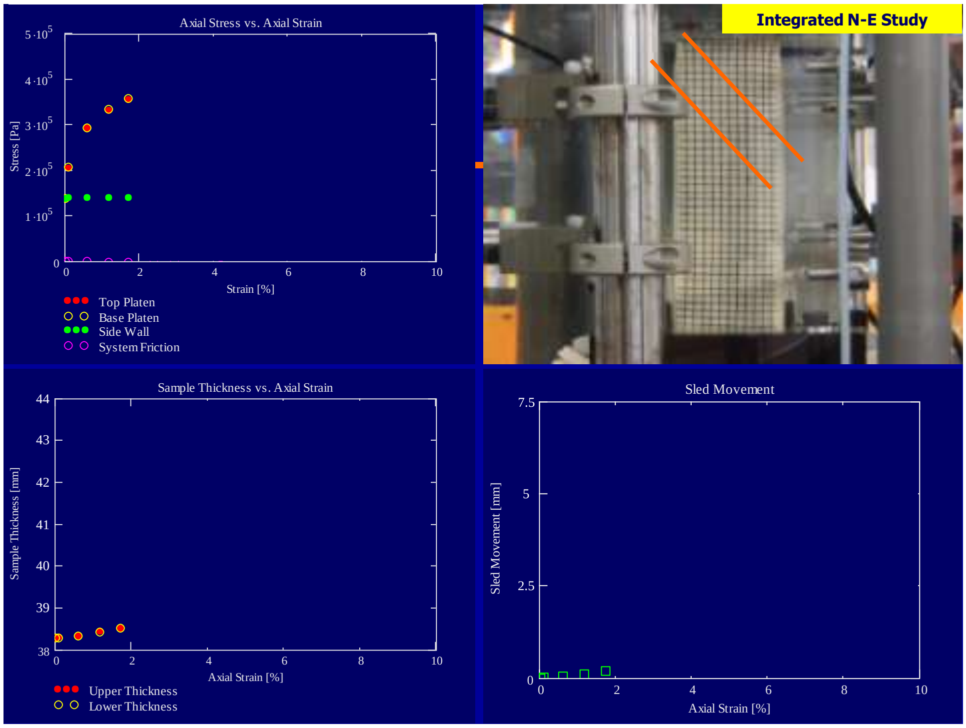
Axial Stress vs. Axial Strain
Stress [Pa]
Strain [%]
Top Platen
Base Platen
Side Wall
System Friction
Integrated N-E Study
Sample Thickness vs. Axial Strain
Sample Thickness [mm]
Axial Strain [%]
Upper Thickness
Lower Thickness
Sled Movement
Sled Movement [mm]
Axial Strain [%]

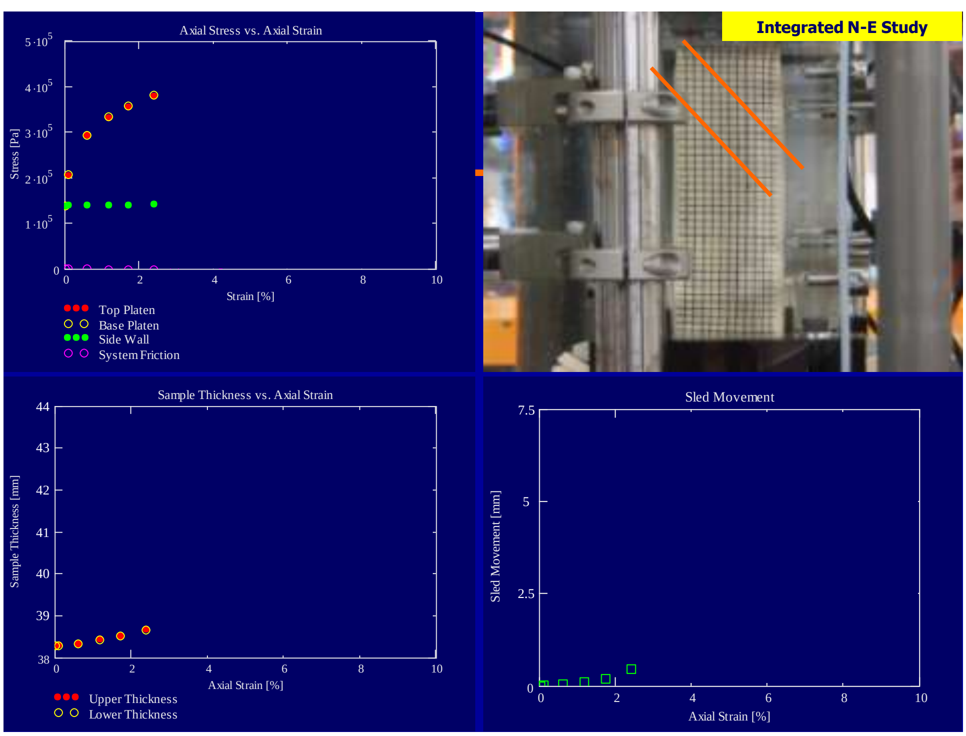
Axial Stress vs. Axial Strain
Stress [Pa]
Strain [%]
Top Platen
Base Platen
Side Wall
System Friction
Integrated N-E Study
Sample Thickness vs. Axial Strain
Sample Thickness [mm]
Axial Strain [%]
Upper Thickness
Lower Thickness
Sled Movement
Sled Movement [mm]
Axial Strain [%]

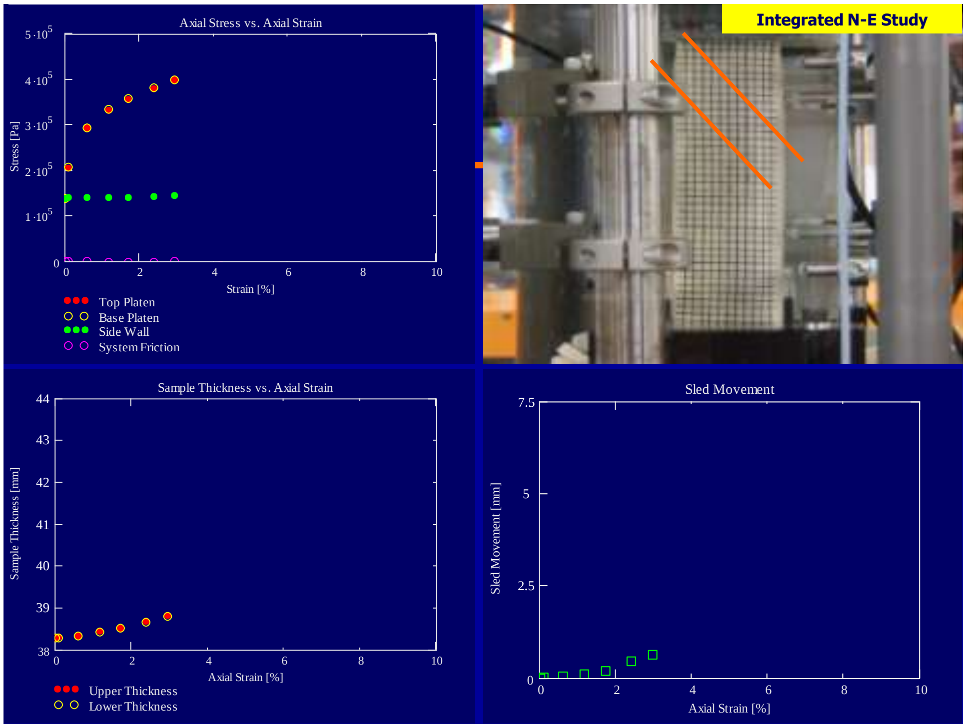
Axial Stress vs. Axial Strain
Stress [Pa]
Strain [%]
Top Platen
Base Platen
Side Wall
System Friction
Integrated N-E Study
Sample Thickness vs. Axial Strain
Sample Thickness [mm]
Axial Strain [%]
Upper Thickness
Lower Thickness
Sled Movement
Sled Movement [mm]
Axial Strain [%]

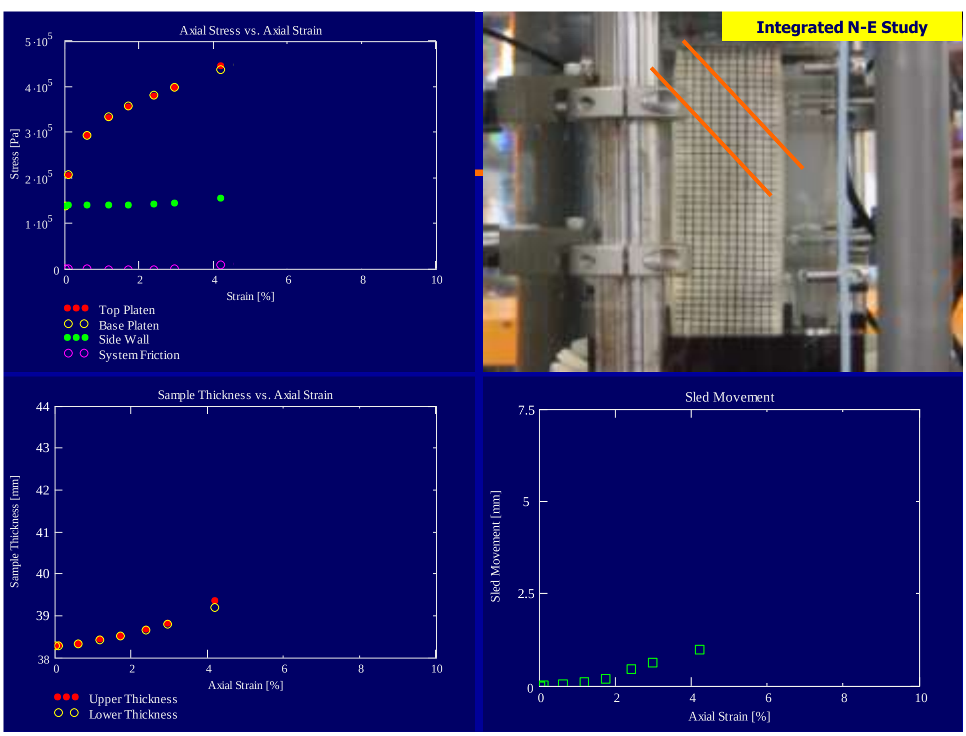
Axial Stress vs. Axial Strain
Stress [Pa]
Strain [%]
Top Platen
Base Platen
Side Wall
System Friction
Integrated N-E Study
Sample Thickness vs. Axial Strain
Sample Thickness [mm]
Axial Strain [%]
Upper Thickness
Lower Thickness
Sled Movement
Sled Movement [mm]
Axial Strain [%]

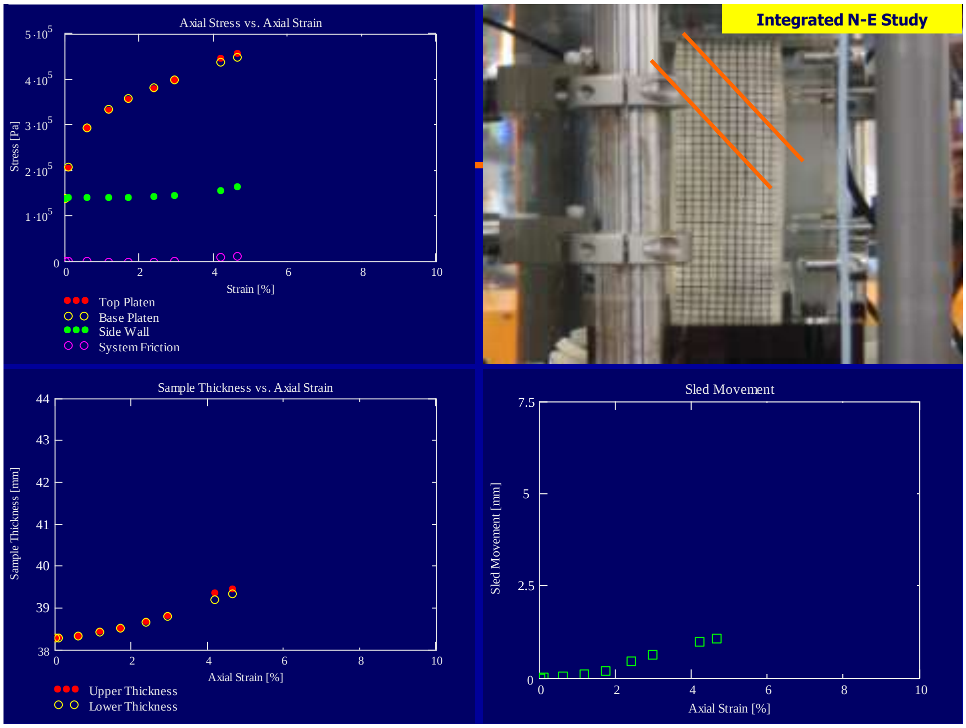
Integrated N-E Study
Axial Stress vs. Axial Strain
Stress [Pa]
Strain [%]
Top Platen
Base Platen
Side Wall
System Friction
Sample Thickness vs. Axial Strain
Sample Thickness [mm]
Axial Strain [%]
Upper Thickness
Lower Thickness
Sled Movement
Sled Movement [mm]
Axial Strain [%]

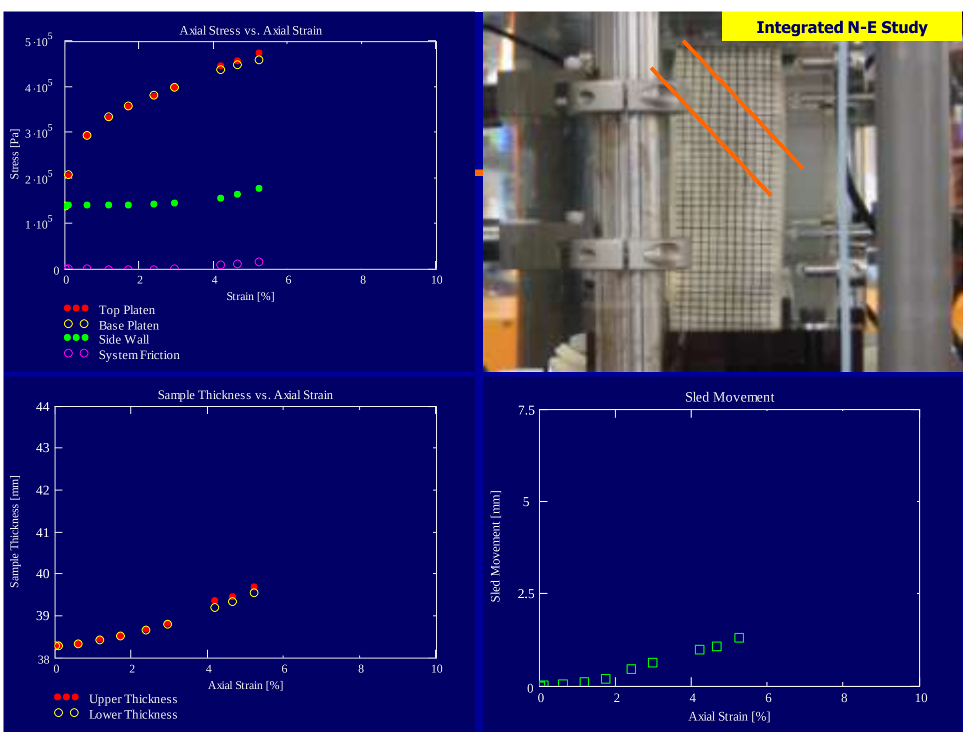
Integrated N-E Study
Axial Stress vs. Axial Strain
Stress [Pa]
Strain [%]
Top Platen
Base Platen
Side Wall
System Friction
Sample Thickness vs. Axial Strain
Sample Thickness [mm]
Axial Strain [%]
Upper Thickness
Lower Thickness
Sled Movement
Sled Movement [mm]
Axial Strain [%]

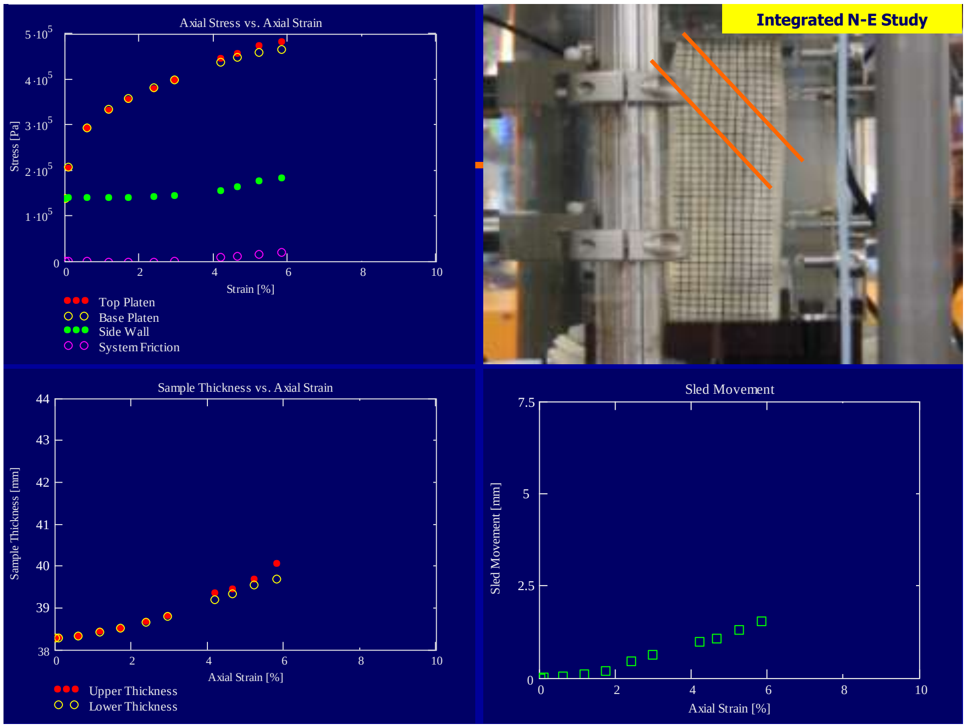
Axial Stress vs. Axial Strain
Stress [Pa]
Strain [%]
Top Platen
Base Platen
Side Wall
System Friction
Integrated N-E Study
Sample Thickness vs. Axial Strain
Sample Thickness [mm]
Axial Strain [%]
Upper Thickness
Lower Thickness
Sled Movement
Sled Movement [mm]
Axial Strain [%]

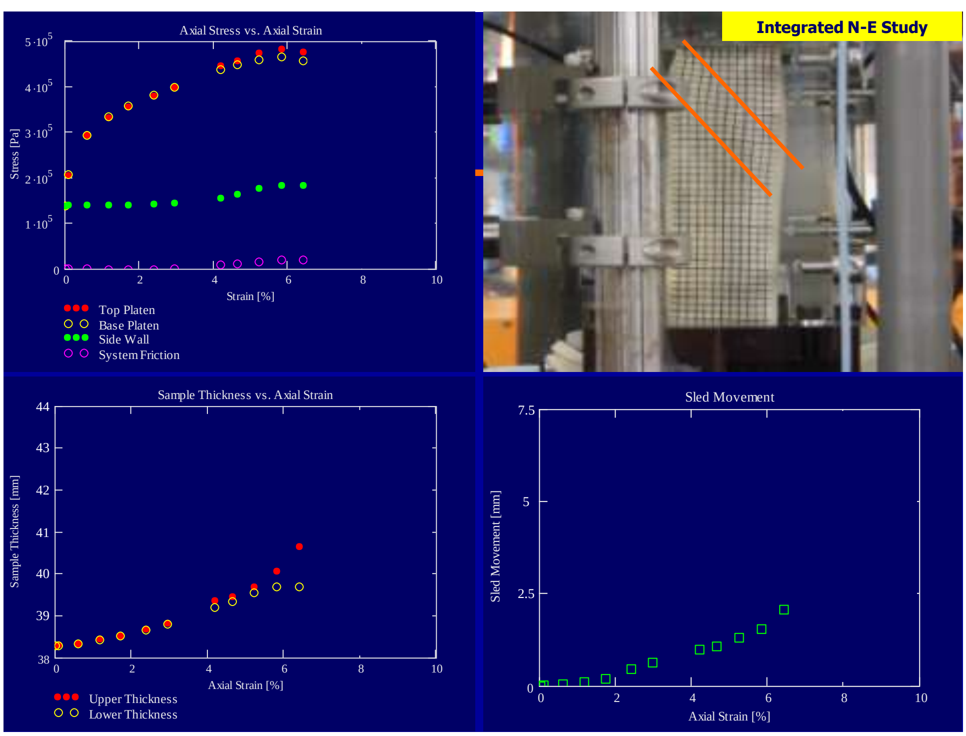
Axial Stress vs. Axial Strain
Stress [Pa]
Strain [%]
Top Platen
Base Platen
Side Wall
System Friction
Integrated N-E Study
Sample Thickness vs. Axial Strain
Sample Thickness [mm]
Axial Strain [%]
Upper Thickness
Lower Thickness
Sled Movement
Sled Movement [mm]
Axial Strain [%]

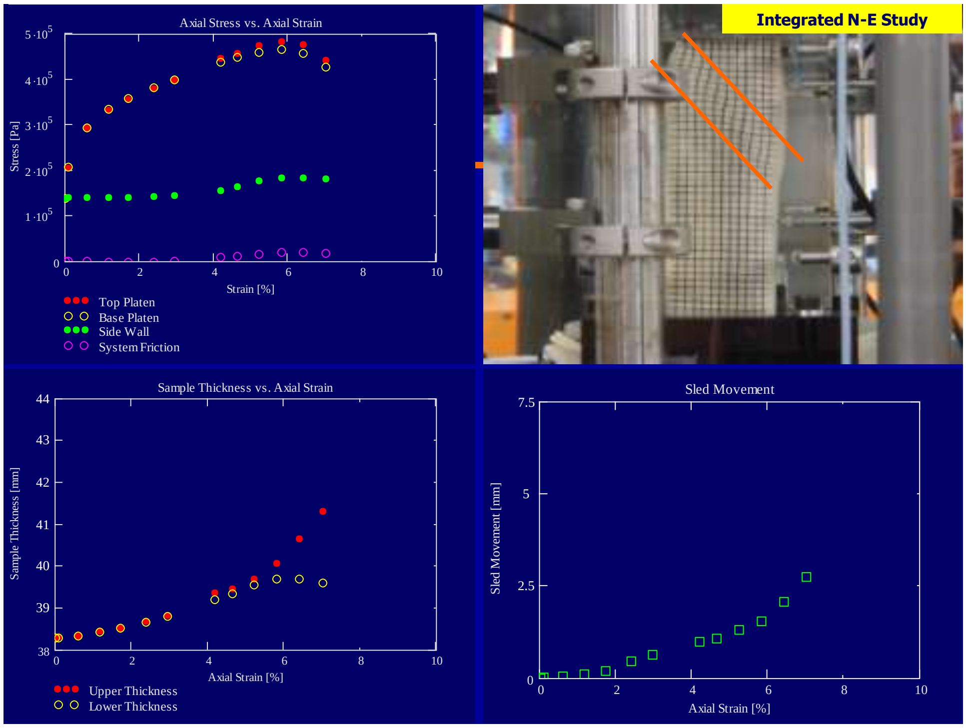
Axial Stress vs. Axial Strain
Stress [Pa]
Strain [%]
Top Platen
Base Platen
Side Wall
System Friction
Integrated N-E Study
Sample Thickness vs. Axial Strain
Sample Thickness [mm]
Axial Strain [%]
Upper Thickness
Lower Thickness
Sled Movement
Sled Movement [mm]
Axial Strain [%]

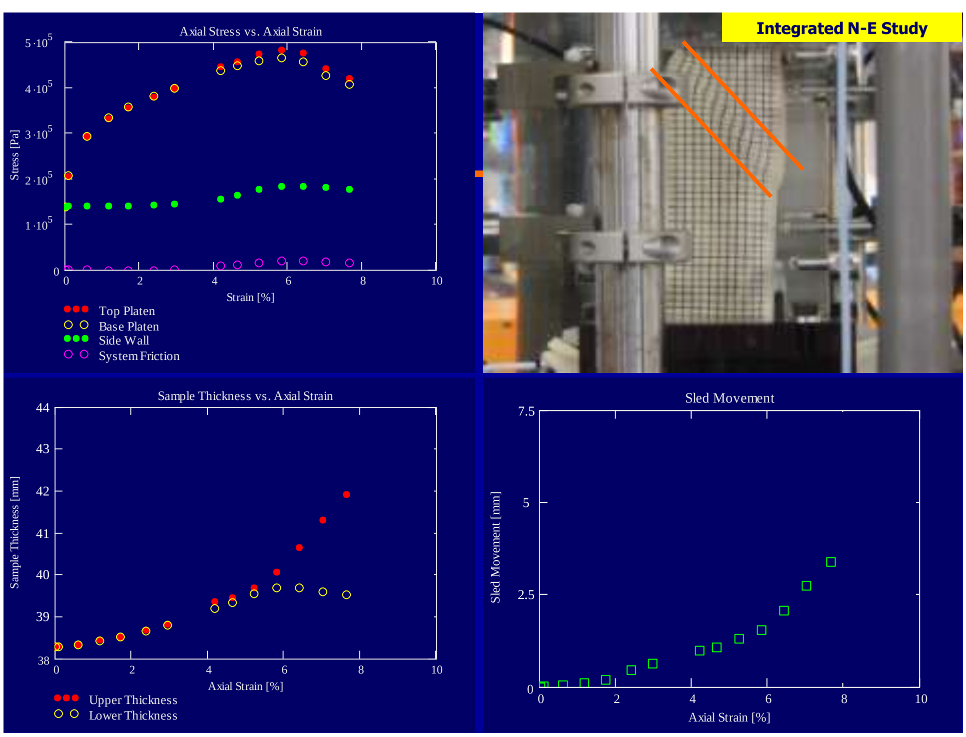
Axial Stress vs. Axial Strain
Stress [Pa]
Strain [%]
Top Platen
Base Platen
Side Wall
System Friction
Integrated N-E Study
Sample Thickness vs. Axial Strain
Sample Thickness [mm]
Axial Strain [%]
Upper Thickness
Lower Thickness
Sled Movement
Sled Movement [mm]
Axial Strain [%]

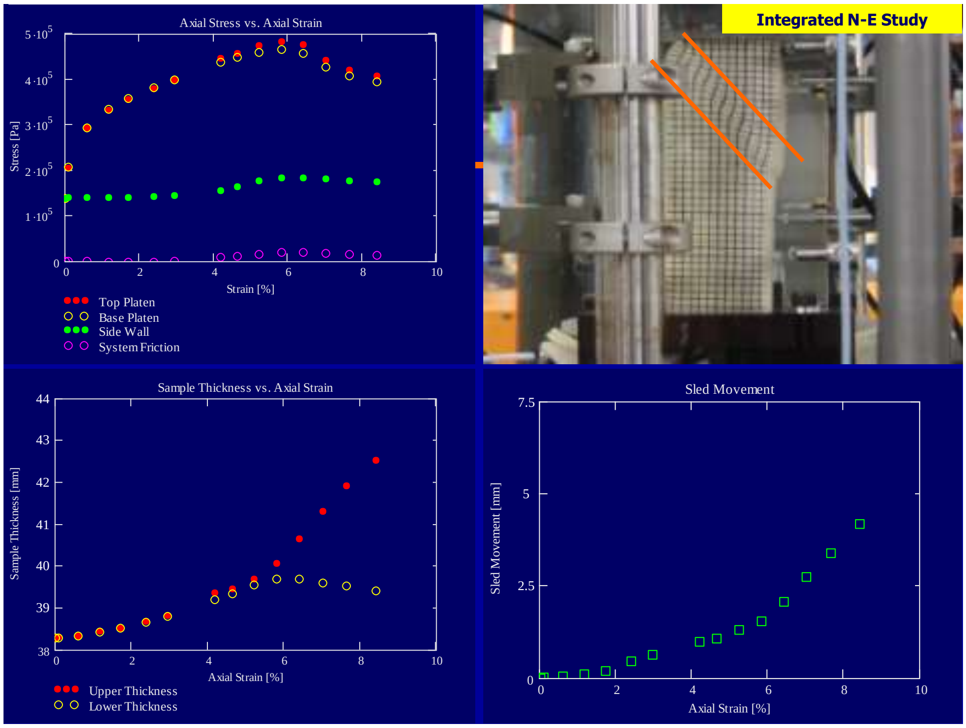
Axial Stress vs. Axial Strain
Stress [Pa]
Strain [%]
Top Platen
Base Platen
Side Wall
System Friction
Integrated N-E Study
Sample Thickness vs. Axial Strain
Sample Thickness [mm]
Axial Strain [%]
Upper Thickness
Lower Thickness
Sled Movement
Sled Movement [mm]
Axial Strain [%]

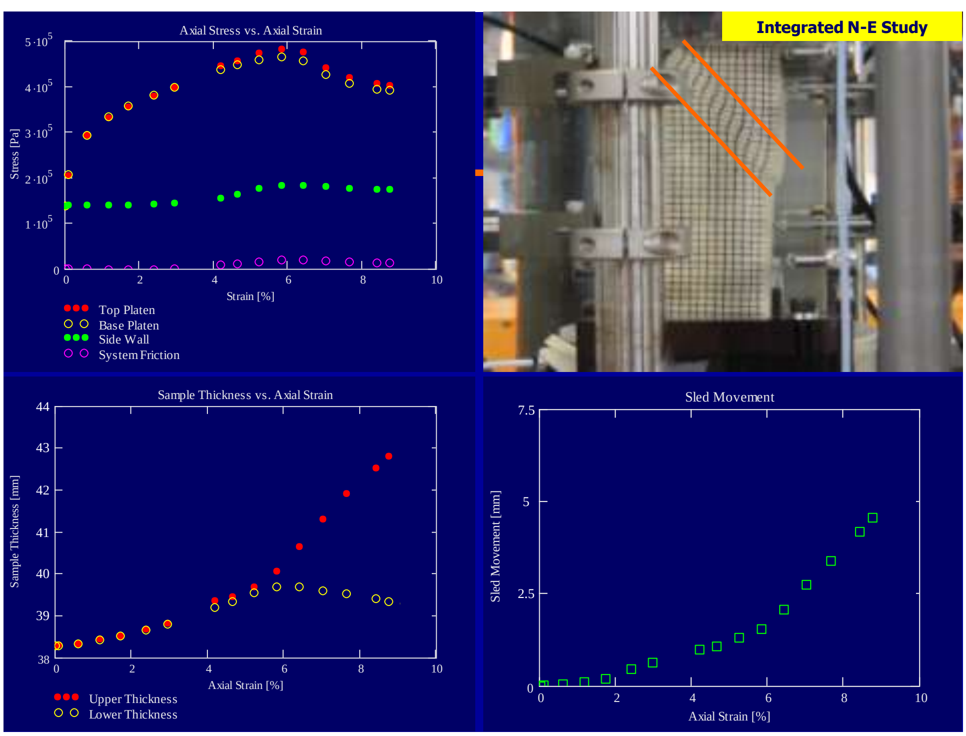
Axial Stress vs. Axial Strain
Stress [Pa]
Strain [%]
Top Platen
Base Platen
Side Wall
System Friction
Integrated N-E Study
Sample Thickness vs. Axial Strain
Sample Thickness [mm]
Axial Strain [%]
Upper Thickness
Lower Thickness
Sled Movement
Sled Movement [mm]
Axial Strain [%]

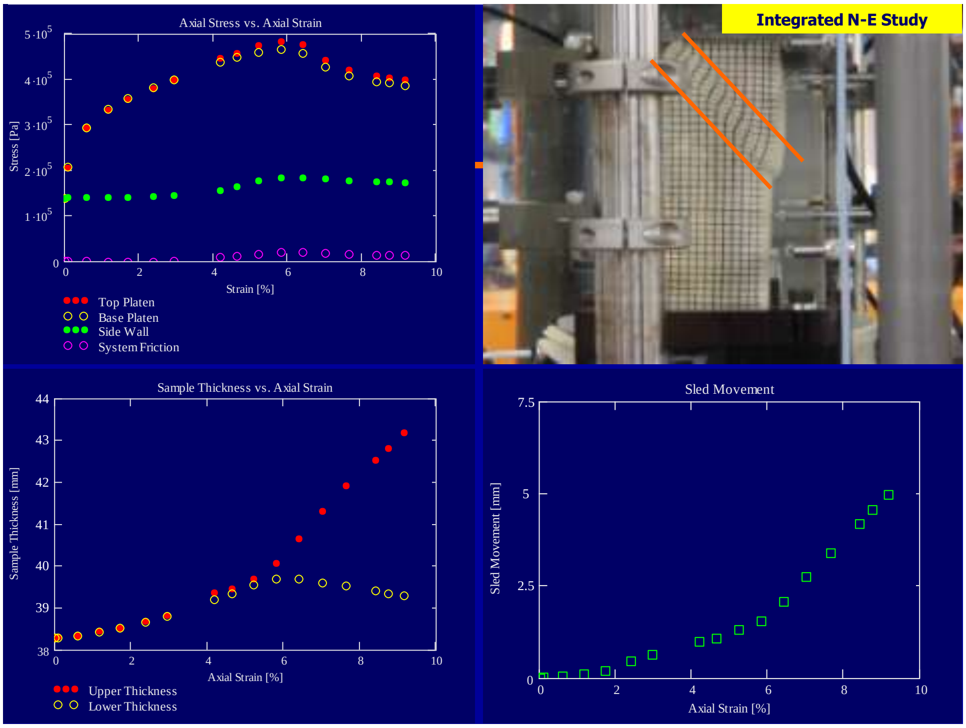
Integrated N-E Study
Axial Stress vs. Axial Strain
Stress [Pa]
Strain [%]
Top Platen
Base Platen
Side Wall
System Friction
Sample Thickness vs. Axial Strain
Sample Thickness [mm]
Axial Strain [%]
Upper Thickness
Lower Thickness
Sled Movement
Sled Movement [mm]
Axial Strain [%]

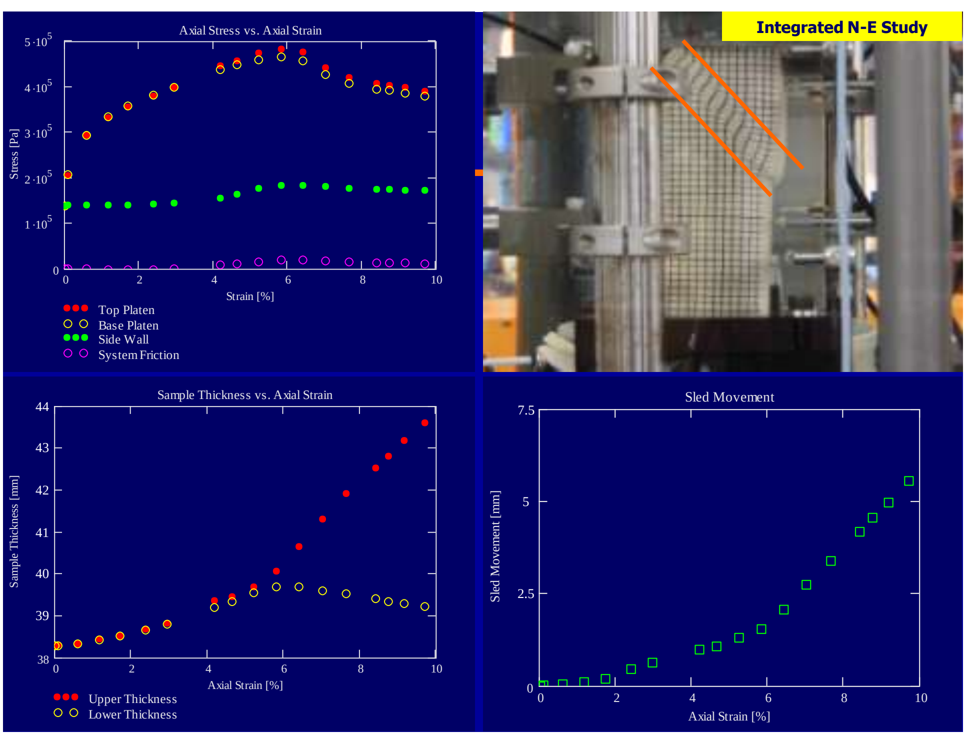
Integrated N-E Study
Axial Stress vs. Axial Strain
Stress [Pa]
Strain [%]
Top Platen
Base Platen
Side Wall
System Friction
Sample Thickness vs. Axial Strain
Sample Thickness [mm]
Axial Strain [%]
Upper Thickness
Lower Thickness
Sled Movement
Sled Movement [mm]
Axial Strain [%]

Biaxial Testing Results

Integrated N-E Study

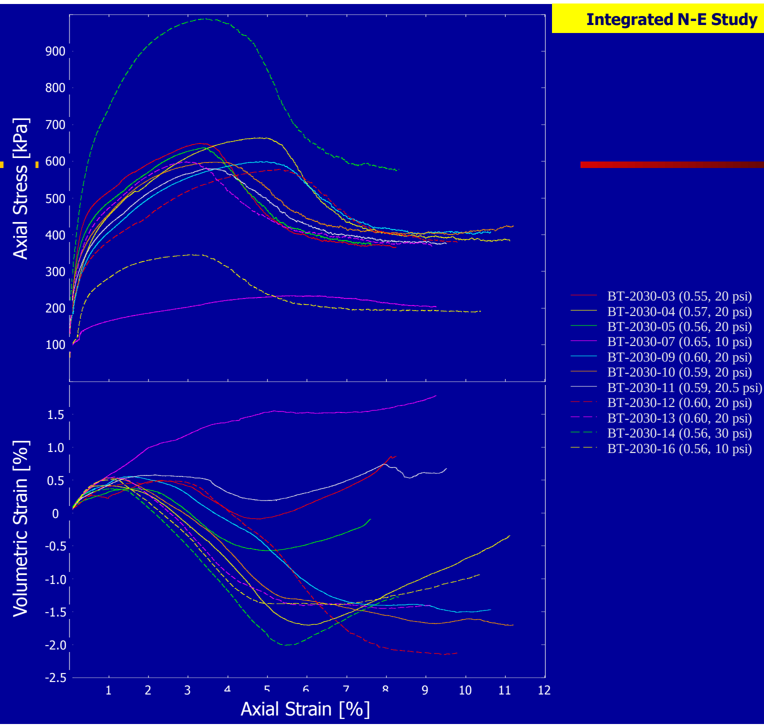

Biaxial Testing Results

Integrated N-E Study

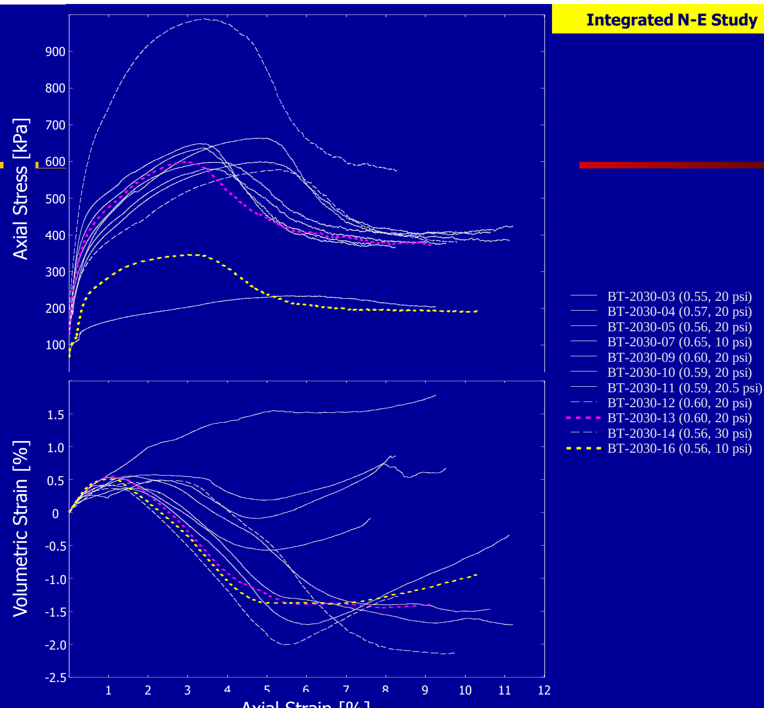

Shear Band Inclination

$$\theta_C = \frac{\pi}{4} + \frac{\phi_p}{2}$$

$$\theta_R = \frac{\pi}{4} + \frac{\psi_p}{2}$$

$$\theta_A = \frac{\pi}{4} + \frac{1}{4}\left(\phi_p + \psi_p\right)$$

Test Designation	ϕ_p	ψ_p	ϕ_{cs}	ϕ_s	ψ_{cs}	θ_e	θ_C	θ_R	θ_A
Slightly dilatant	38.8°	8.8°	27.7°	27.7°	1.0°	59°	64°	49°	57°
Highly dilatant	41.8°	11.5°	27.9°	27.9°	0.2°	61°	66°	51°	58°

Integrated N-E Study

Specimen Impregnation and Sectioning

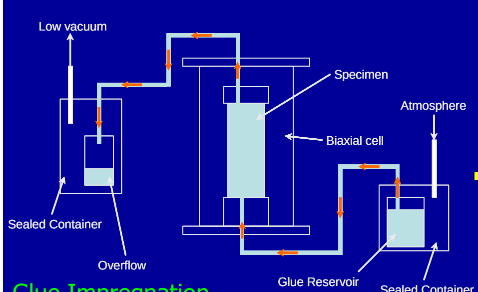

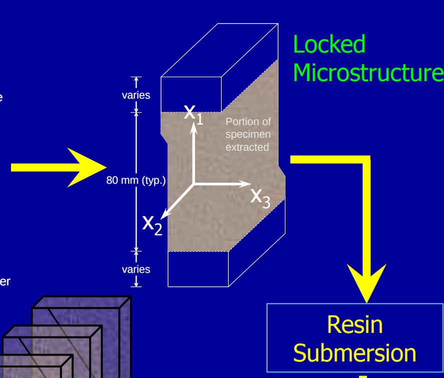

Solidified and Sectioned

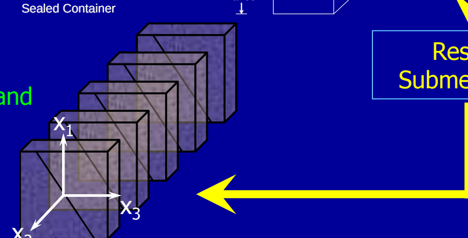

Surfaces for imaging are on the negative x_2 plane

Integrated N-E Study

Surface Preparation and Image Capture

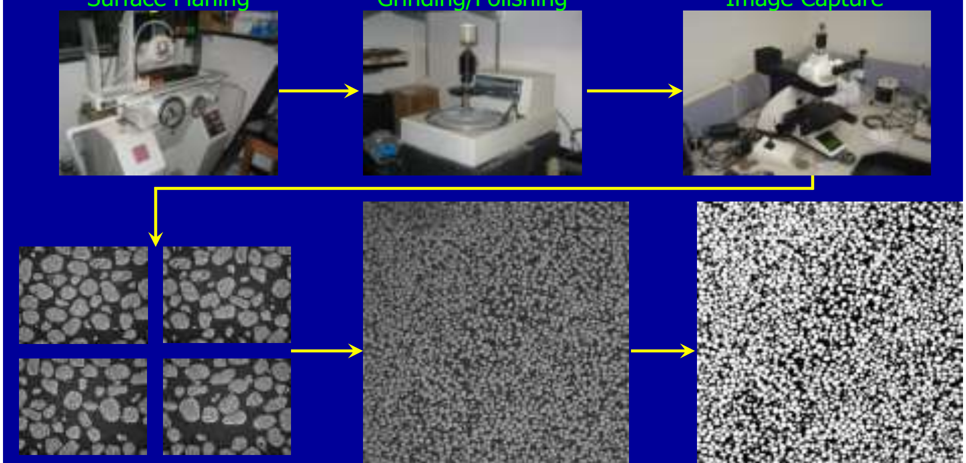

Integrated N-E Study

Local Void Ratios

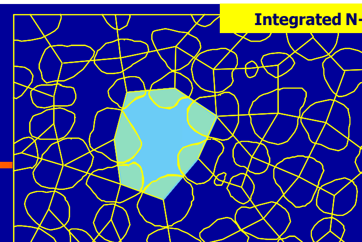

(after Park, 1999)

Area of solid Particles, A_s

Area of Voids, A_v

Local Void Ratio = A_v/A_s

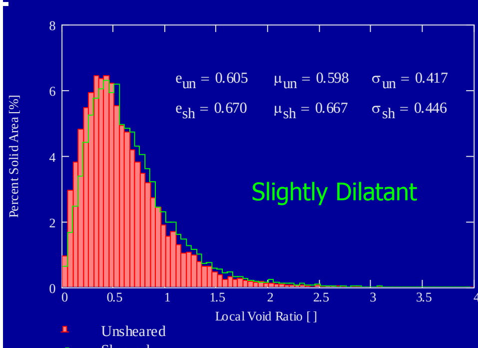

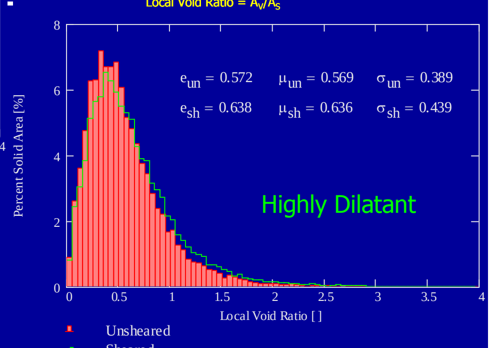

Shearing tends to flatten the histogram and shift it to the right

Void Ratio Distributions

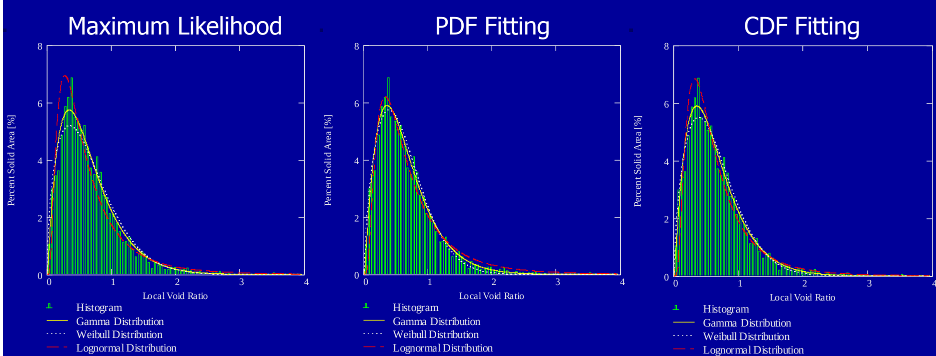

Microscale Experimental Results

Subregional Analyses

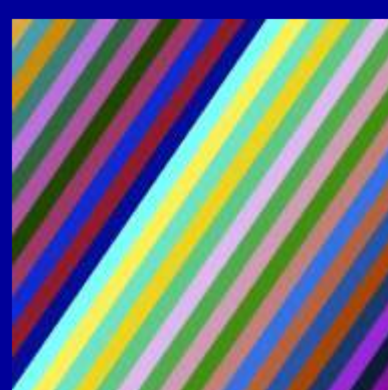

Strip Analyses

Integrated N-E Study

Void Ratio Contours

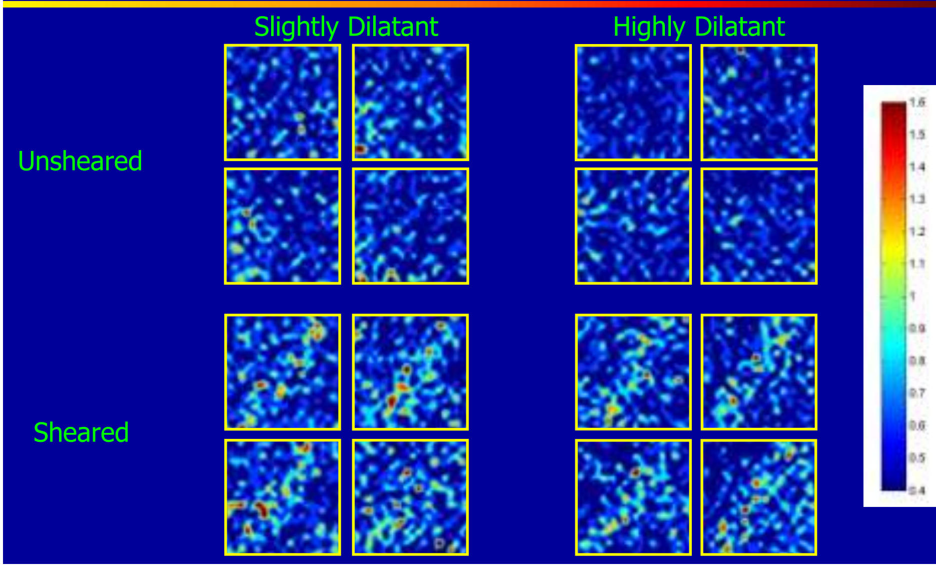

Integrated N-E Study

Strip Analyses

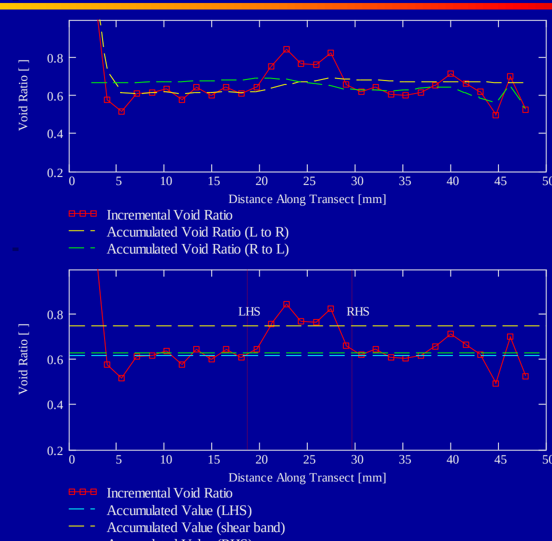

Strip Analyses

Slightly Dilatant | Highly Dilatant

Unsheared

Sheared

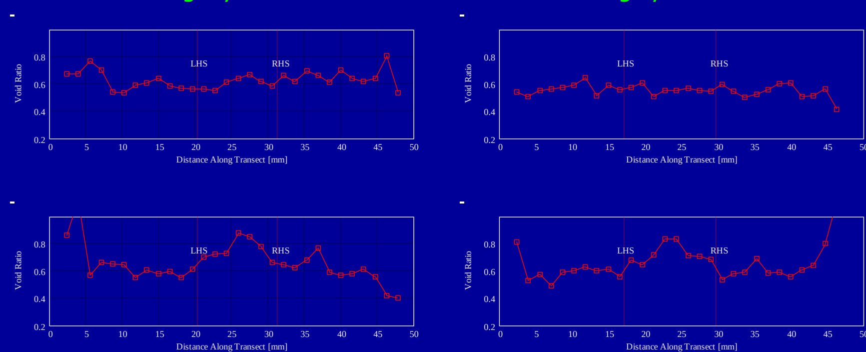

Strip Analyses: LVRD

Slightly Dilatant | Highly Dilatant

Unsheared

Sheared

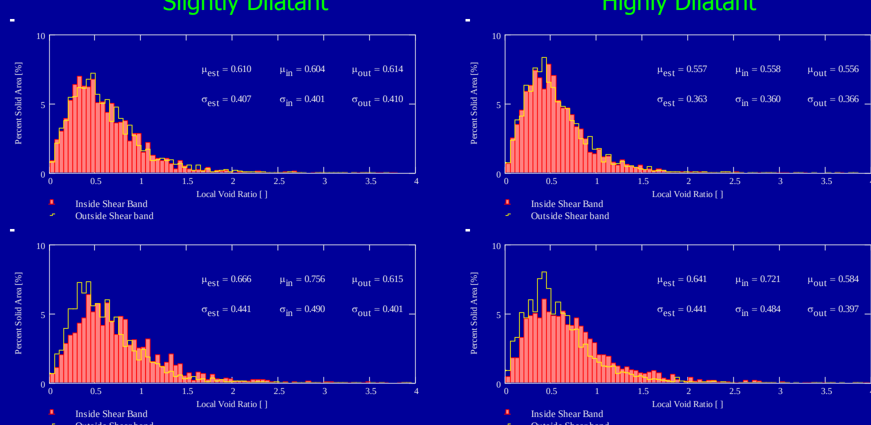

LVRD Statistics

	Mean (μ_{est})	Standard Deviation (σ_{est})
Slightly Dilatant Specimen		
Unsheared	0.598	0.417
Sheared	0.667 (11.1%)	0.444
Inside Shear Band	0.747 (24.6%)	0.490
Outside Shear Band	0.622 (3.6%)	0.409
Highly Dilatant Specimen		
Unsheared	0.569	0.389
Sheared	0.636 (13.6%)	0.439
Inside Shear Band	0.715 (27.6%)	0.482
Outside Shear Band	0.588 (4.9%)	0.403

Distribution entropy: $H_V = -\sum_{i=1}^{n} P_i \cdot \log_n(P_i)$

Integrated N-E Study

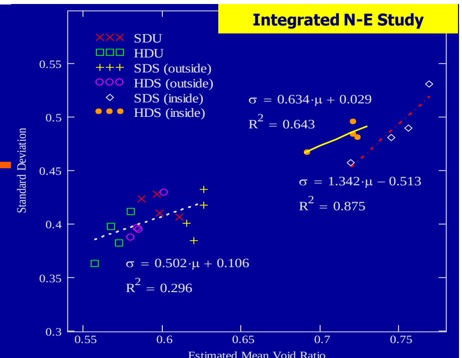

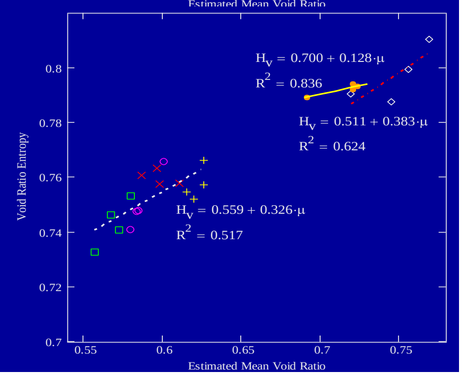

Gamma Distributions

Integrated N-E Study

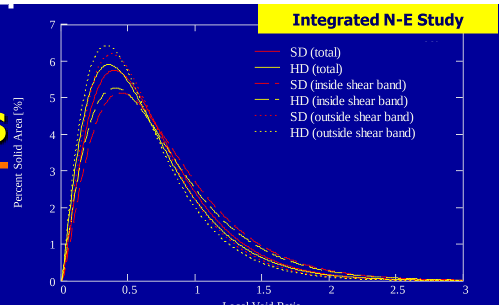

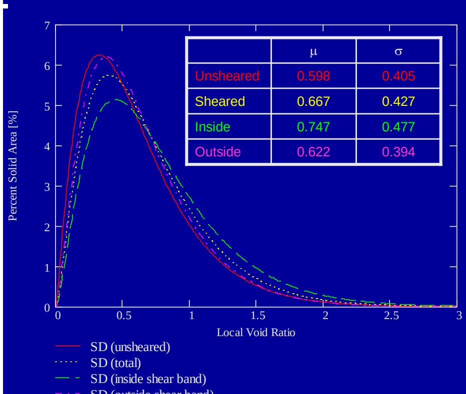

	μ	σ
Unsheared	0.598	0.405
Sheared	0.667	0.427
Inside	0.747	0.477
Outside	0.622	0.394

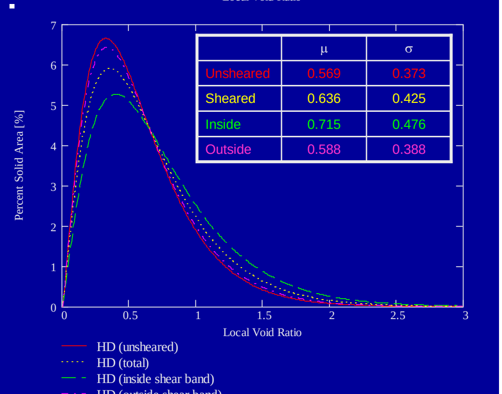

	μ	σ
Unsheared	0.569	0.373
Sheared	0.636	0.425
Inside	0.715	0.476
Outside	0.588	0.388

Critical State

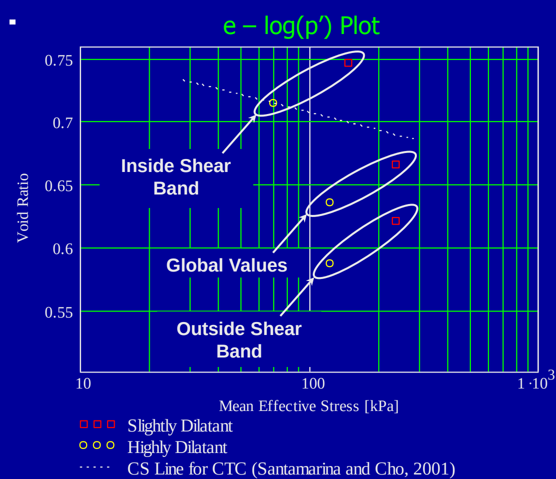

Above and Below the Shear Band

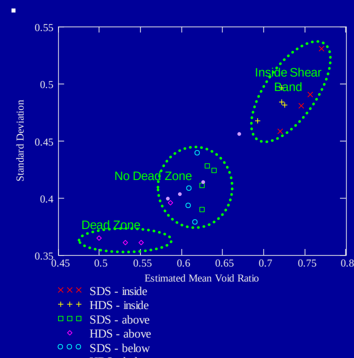

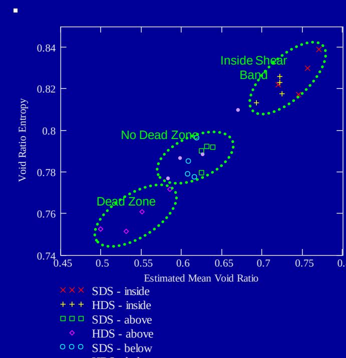

Side View

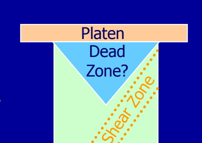

Plan View

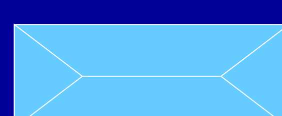

Shear Band Thickness

	Slightly Dilatant		Highly Dilatant	
	(mm)	(d_{50})	(mm)	(d_{50})
Void ratio strips				
20	11.0	15	12.5	17
40	9.4	13	11.0	15
60	11.0	15	12.5	17
80	12.5	17	11.0	15
Virtual surfaces	5.9	8	7.8	11
Image measurement				
20	8.7	12	8.4	11
40	8.5	11	9.7	13
60	9.4	13	9.2	12
80	7.6	10	9.7	13
External measurement	8.3	11	9.0	12

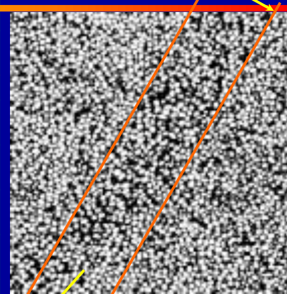

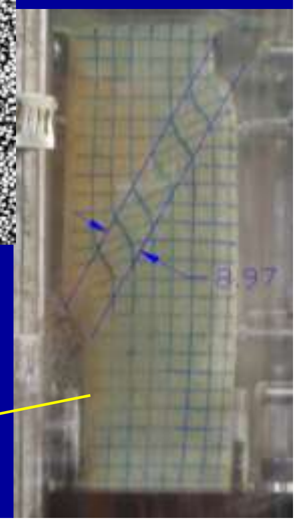

Integrated N-E Study

The Transition Zone Concept

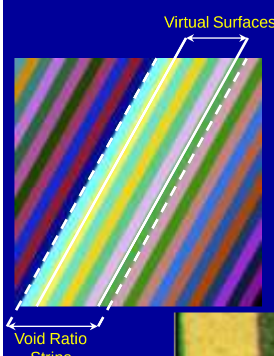

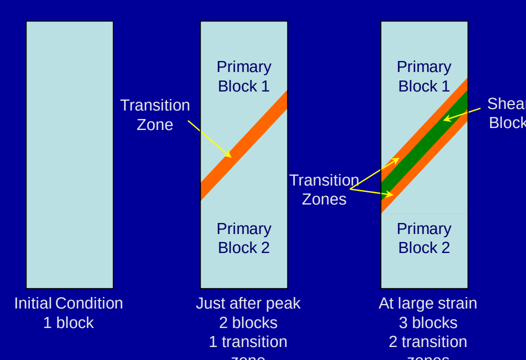

Integrated N-E Study

Numerical Simulations

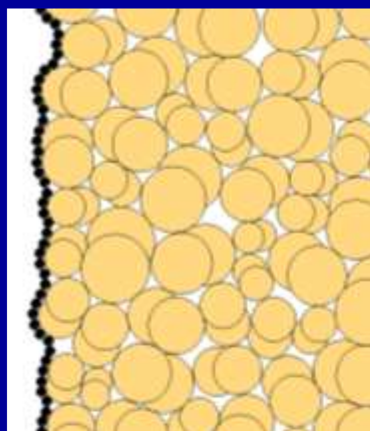

Velocity-Controlled Flexible Wall

Parameter	Numerical Simulations	Physical Comparison	Reference
Particle normal stiffness	10^8 N/m	4×10^6 N/m	(Santamarina et al., 2001)
Particle shear stiffness	10^7 N/m	n/a	n/a
Particle friction coefficient	0.31	0.31	(Proctor and Barton, 1974)
Particle specific gravity	2.65	2.65	(Yang, 2002)
Platen stiffness	10^8 N/m	n/a	n/a
Membrane stiffness	10^7 N/m	500 N/m	(Frost, 1989)
Platen/membrane friction coefficient	0.31	n/a	n/a
Membrane specific gravity	1.50	1.10	(MatWeb, 2005)

Integrated N-E Study

Numerical-Experimental Comparison

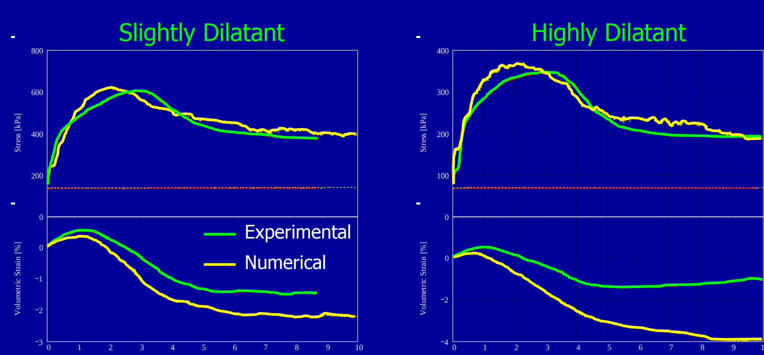

Test Designation	ϕ_p	ψ_p	ϕ_{cs}	ϕ_s	ψ_{cs}	θ_e	θ_C	θ_R	θ_A
SD (E)	38.8°	8.8°	27.7°	27.7°	1.0°	59°	64°	49°	57°
SD (N)	39.5°	16.7°	28.3°	28.2°	3.0°	57°	65°	53°	59°
HD (E)	41.8°	11.5°	27.9°	27.9°	0.2°	61°	66°	51°	58°
HD (N)	42.8°	9.5°	27.8°	27.8°	3.8°	58°	66°	50°	58°

Integrated N-E Study

Shear Band Formation

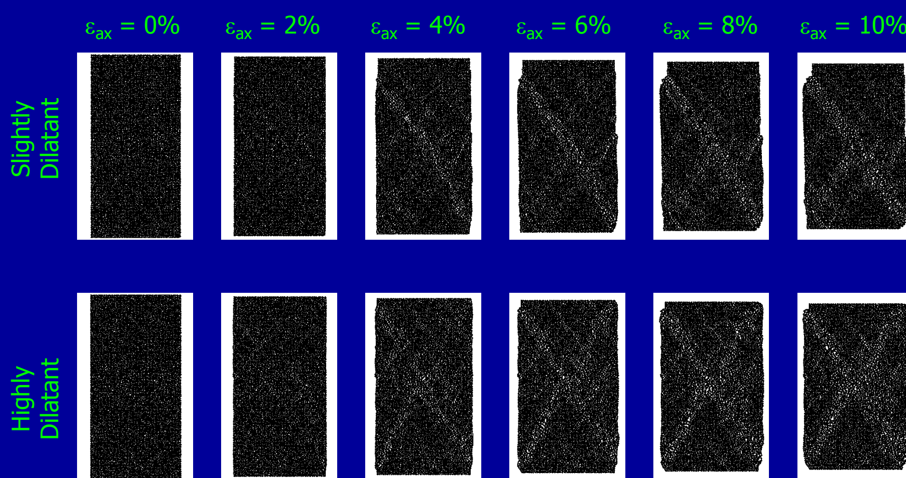

Integrated N-E Study

Subregional Void Ratio Analyses

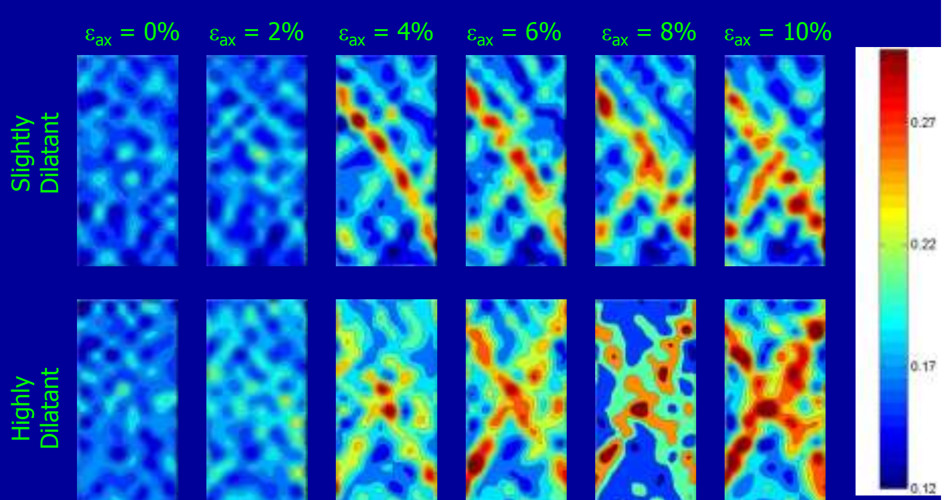

Integrated N-E Study

Evolution of LVRD

Slightly Dilatant

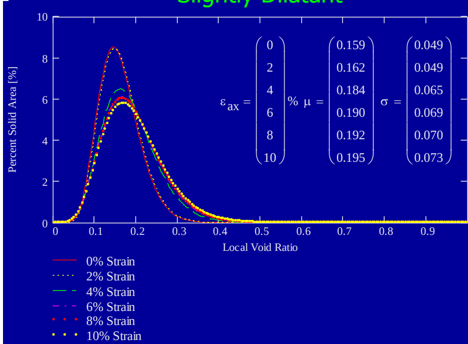

Highly Dilatant

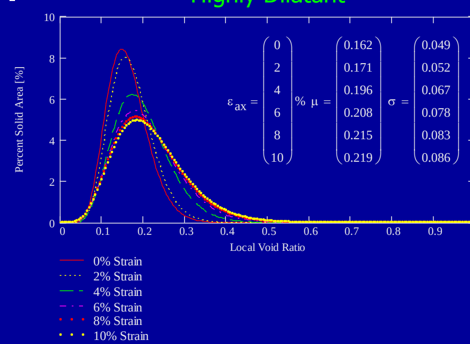

Integrated N-E Study

Numerical Results: Strip Analyses

Slightly Dilatant

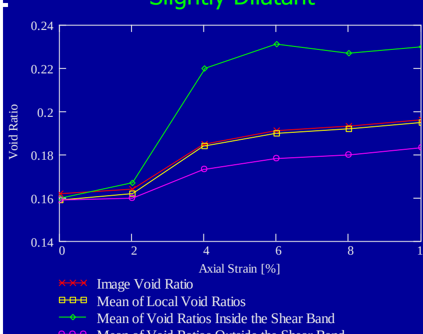

Highly Dilatant

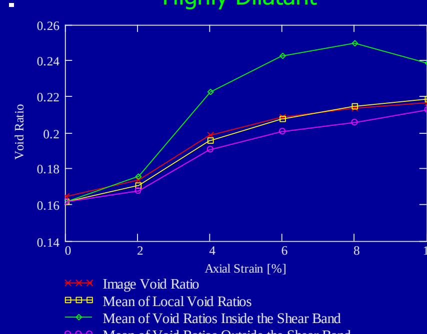

Integrated N-E Study

Shear Band Parameters

	Void Ratio Strips		Direct Measurement	
	(L)	(d_{50})	(L)	(d_{50})
Slightly Dilatant Specimen				
ε_{ax} = 4%	0.97	15	0.91	15
ε_{ax} = 6%	0.97	15	0.97	15
ε_{ax} = 8%	1.1	18	1.1	18
ε_{ax} = 10%	1.1	18	1.3	21
Highly Dilatant Specimen				
ε_{ax} = 4%	0.65	10	0.99	16
ε_{ax} = 6%	0.65	10	0.99	16
ε_{ax} = 8%	0.81	12	1.1	18
ε_{ax} = 10%	0.97	15	1.2	19

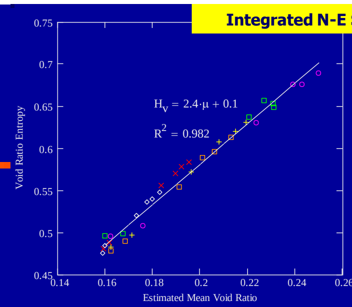

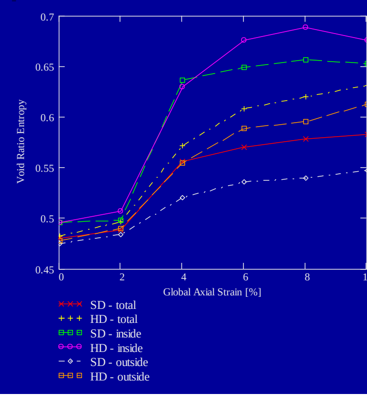

Preliminaries

Overview

- Soil micromechanics
- Discrete element method (DEM)
- Integrated Numerical-Experimental Study
- DEM Simulations: Effects of Geometry
- Soil-Structure Interaction (SSI)
- Thermal Conductivity
- Summary and Conclusions

Simulation of Laboratory Tests

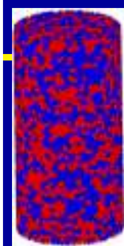

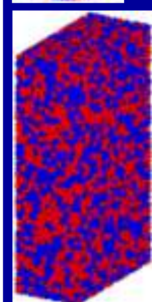

- Assemblies consisted of ~15,000 2-ball particles in the sample volume
  - 2H:1W for axisymmetric
  - 7H:2W:4D for plane strain
- Specimens assembled in "loose" (e_0 = 0.67), "medium" (e_0 = 0.54), and "dense" (e_0 = 0.47) states
- Consolidated under "low" (σ_3' = 75 kPa) and "high" (σ_3' = 450 kPa) confining stresses
- Stacked wall entities used for servo control of confining stresses
- Model and material parameters constant across simulations

Zhao, X. and T.M. Evans. (2009). "Discrete Simulations of Laboratory Loading Conditions," *International Journal of Geomechanics*, 9(4), pp. 169-178.

Macroscale Simulation Results

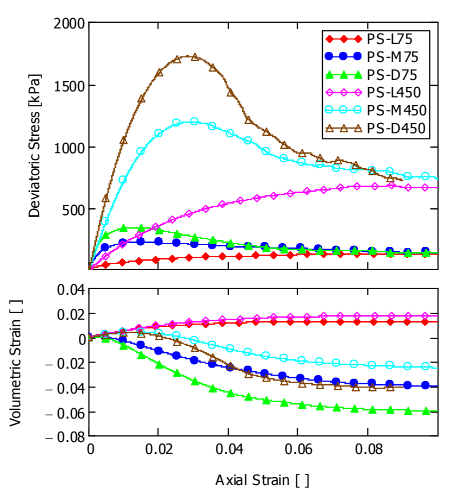

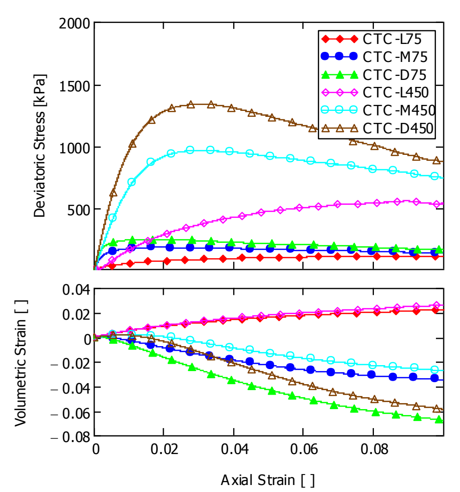

Plane Strain Simulations

- Note effects of e_0 and σ_3'
- Convergence to ultimate/terminal state (=f(e_0))

Axisymmetric Simulations

- Effects of e_0 and σ_3' similar to PS
- No ultimate/terminal state at ε_1=10%

Macroscale Deformation

Plane Strain | Axisymmetric Compression

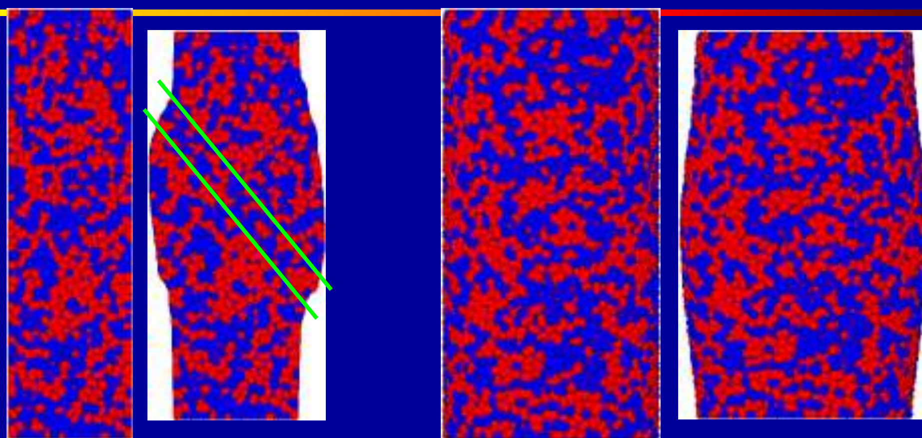

Plane Strain Simulations

- Region of high localized strain (shear band)
- Post-peak stress-strain response controlled by shear band

Axisymmetric Simulations

- Diffuse (bulging) failure, single shear band not easily identified
- Entire specimen still deforming post-peak

Effects of Geometry

Small-Strain Response

Young's Modulus: Calculated from CTC Results versus Measured in PS

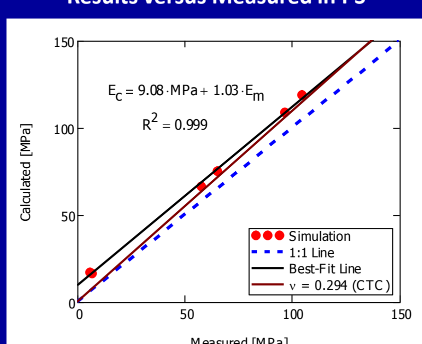

$$E_{PS} = \frac{E_{CTC}}{1-\nu_{CTC}^2}$$

Poisson's Ratio: Calculated from CTC Results versus Measured in PS

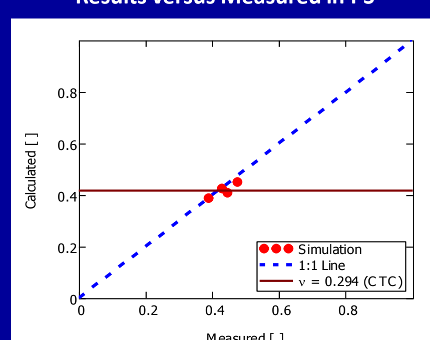

$$\nu_{PS} = \frac{\nu_{CTC}}{1-\nu_{CTC}}$$

Shear Strength

Rowe (1962)

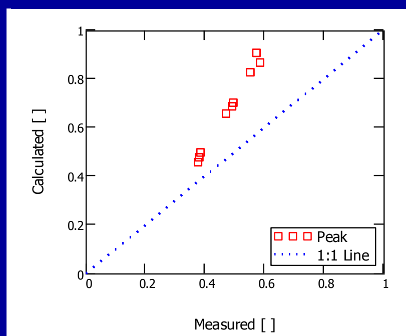

$$\tan\phi'_{ds} = \tan\phi'_{ps}\cos\phi'_{cv}$$

Bolton (1986)

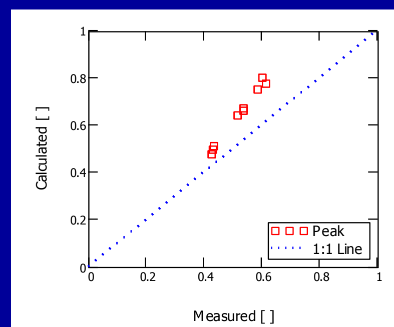

$$\phi'_{ps} = \tan^{-1}(1.2\tan\phi'_{ds\,sec})$$

Shear Strength

Ramamurthy and Tokhi (1981)

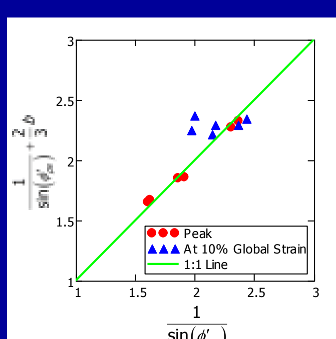

b = $(\sigma_2'-\sigma_3')/(\sigma_1'-\sigma_3')$

Hanna (2001)

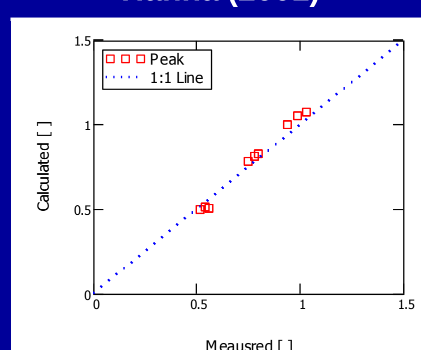

$$\tan\phi'_{ps}\cos\phi'_{cv} = \frac{(KD-1)\sqrt{12D-3D^2}}{4KD-KD^2+3D}$$

$$D = 1-\frac{d\upsilon}{d\varepsilon_1} \qquad K = \tan^2\left(45° + \frac{\phi'_{cv}}{2}\right)$$

- Peak strength is consistent with the theoretical relationship of R&T (1981) and Hanna (2001)
- Results at ultimate strain are inconsistent, with the exception of specimens which do not dilate

Friction and Dilation

Bolton's (1986) Dilatancy Relationships (note that black points are TXC)

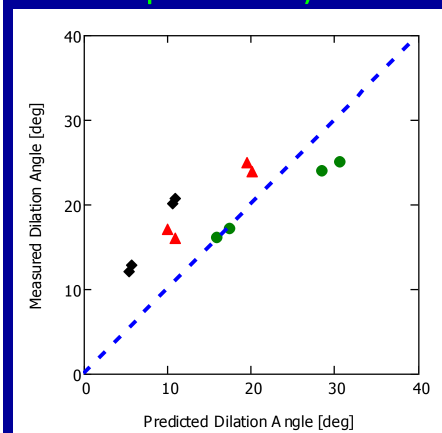

$$\psi_p = 10\left(-\frac{d\varepsilon_v}{d\varepsilon_1}\right)_{max}$$

$$\psi_p = \frac{1}{0.048}\left(-\frac{d\varepsilon_v}{d\varepsilon_1}\right)_{max}$$

$$\psi_p = 1.25\left(\varphi'_p - \varphi'_{cs}\right)$$

- Dilation angle measurements are not strictly consistent with the semi-empirical relationships of Bolton
- In general, boundary measurements will tend to overpredict the dilation angle

Overview

- Soil micromechanics
- Discrete element method (DEM)
- Integrated Numerical-Experimental Study
- DEM Simulations: Effects of Geometry
- Soil-Structure Interaction (SSI)
- Thermal Conductivity
- Summary and Conclusions

Definition of the Granular Material

Material Properties:

Parameter	Numerical Simulation	Physical Comparison	Reference
Grain Normal Stiffness	10^8 N/m	4×10^6 N/m	(Santamarina et al., 2001)
Grain Shear Stiffness	10^7 N/m	n/a	n/a
Grain Friction	0.31	0.31	(Proctor and Barton, 1974)
Grain Specific Gravity	2.65	2.65	(Yang, 2002)
Wall Stiffness	10^8 N/m	n/a	n/a

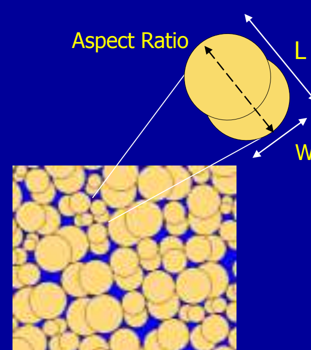

Soil-Structure Interaction

Shear Strength of the Granular Material

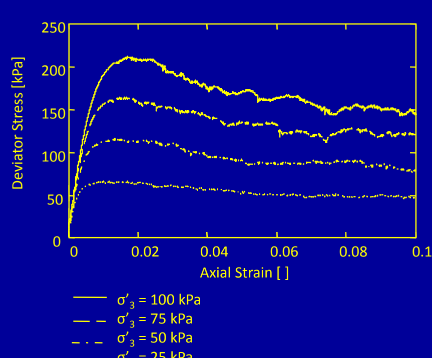

Biaxial Compression Deviator Stress

Friction Value for Confining Stress Cases

Confining Stress (kPa)	Peak Friction Angle (deg)	Critical State Friction Angle (deg)
25	34.8	28.8
50	32.5	26.3
75	31.6	26.6
100	31.0	24.9
Mean	32.5	26.6

Soil-Structure Interaction

Shear Strength of the Granular Material

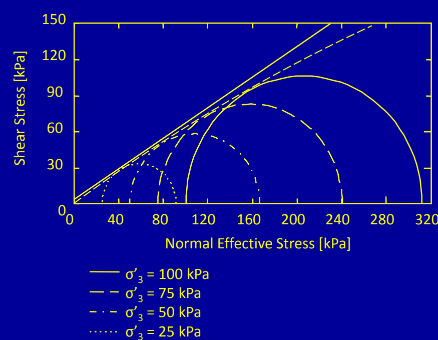

Mohr-Coulomb Method at Peak

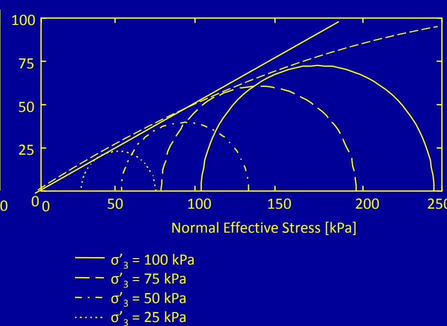

Mohr-Coulomb Method at Critical State

Soil-Structure Interaction

Elastic Properties of the Granular Material

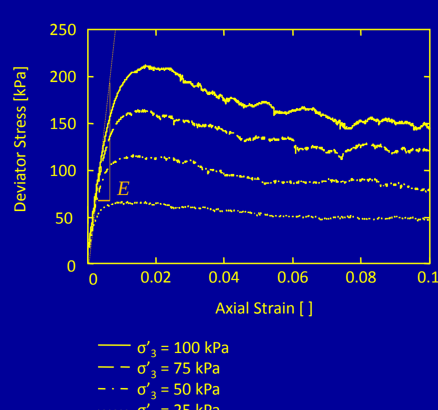

Initial Elastic Region of the Deviator Strain Curve

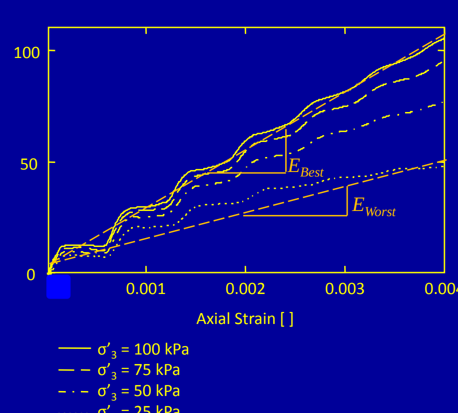

Small Strain Region of the Deviator Strain Curve

Soil-Structure Interaction

Elastic Properties of the Granular Material

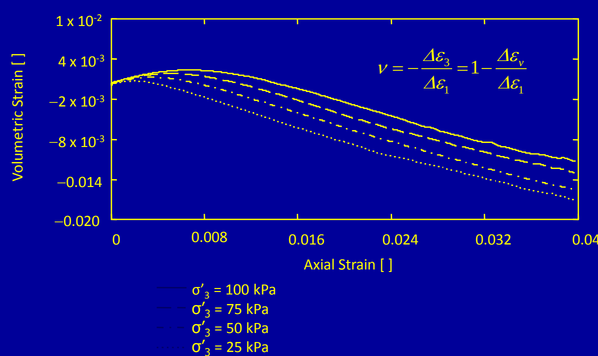

Biaxial Compression Volumetric Strain

Soil-Structure Interaction

Elastic Properties of the Granular Material

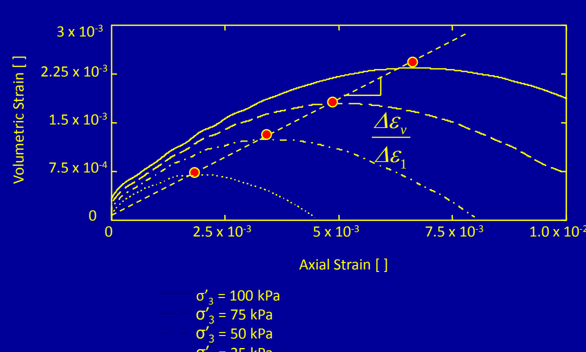

Biaxial Compression Volumetric Strain

Interface Strength of the Granular Material

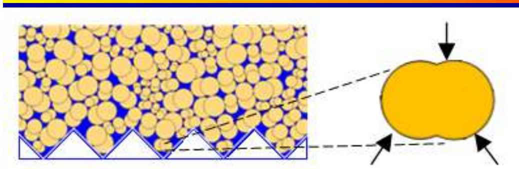

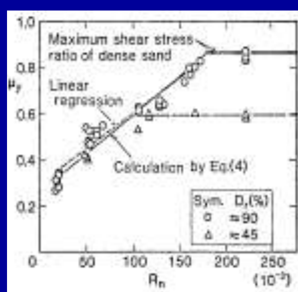

Coefficient of Friction Experimental Results (after Uesugi & Kishida 1986b)

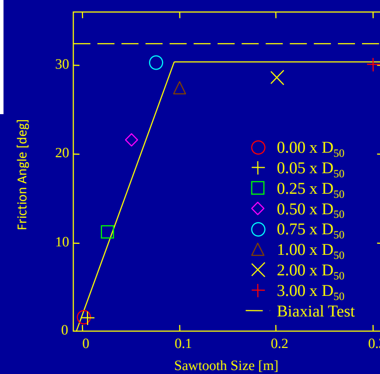

DEM Interface Shear Results for Friction Angle

Soil-Structure Interaction

Shallow Foundation Models

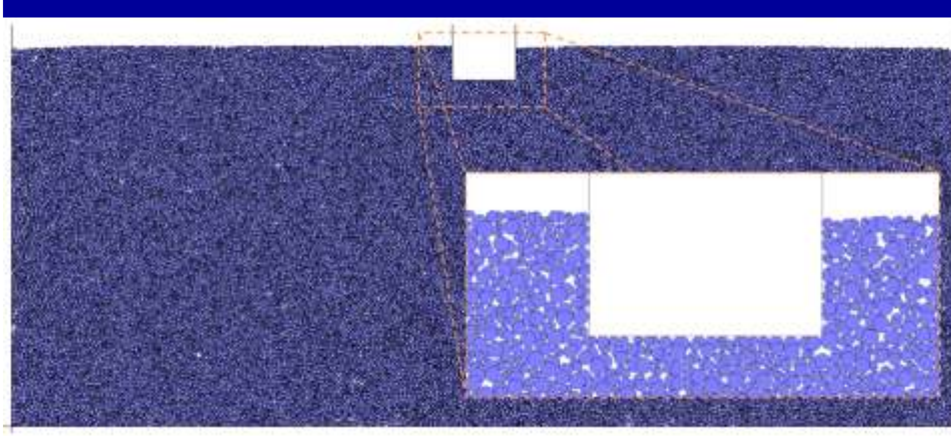

Soil-Structure Interaction

Shallow Foundation Models

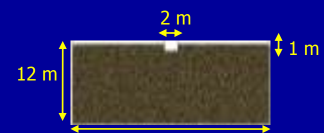

Shallow Foundation Baseline Assembly

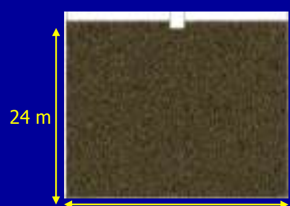

Shallow Foundation Extended Height Assembly

Shallow Foundation Extended Width Assembly

Soil-Structure Interaction

Shallow Foundation Results

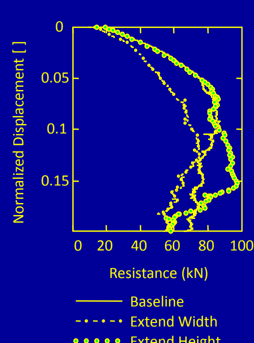

Shallow Foundation Model Dimensions Total Resistance

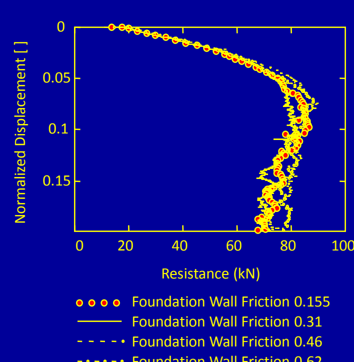

Shallow Foundation Friction Total Resistance

Shallow Foundation Results

δ = 0.00B

Shallow Foundation Grain Rotations at 0.00B, Vertical Displacement

Rotations Color Bar for Rotations Figures (deg)

Soil-Structure Interaction

Shallow Foundation Results

δ = 0.05B

Shallow Foundation Grain Rotations at 0.05B, Vertical Displacement

Rotations Color Bar for Rotations Figures (deg)

Shallow Foundation Results

δ = 0.10B

Shallow Foundation Grain Rotations at 0.10B, Vertical Displacement

Rotations Color Bar for Rotations Figures (deg)

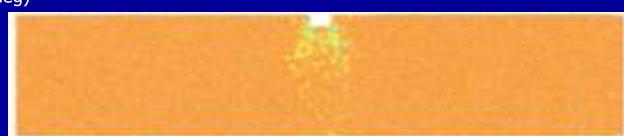

Soil-Structure Interaction

Shallow Foundation Results

δ = 0.15B

Shallow Foundation Grain Rotations at 0.15B, Vertical Displacement

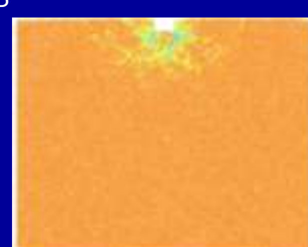

Rotations Color Bar for Rotations Figures (deg)

Shallow Foundation Results

$\delta = 0.20B$

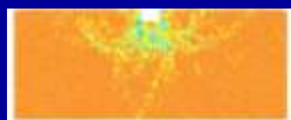

Shallow Foundation Grain Rotations at 0.20B, Vertical Displacement

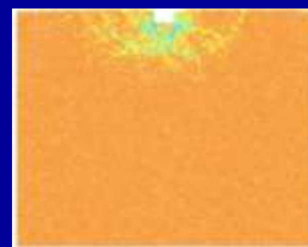

Rotations Color Bar for Rotations Figures (deg)

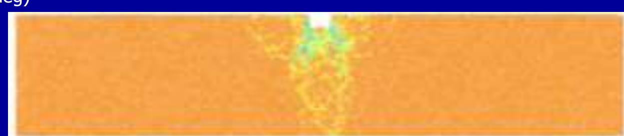

Shallow Foundation Results

$\delta = 0.25B$

Shallow Foundation Grain Rotations at 0.25B, Vertical Displacement

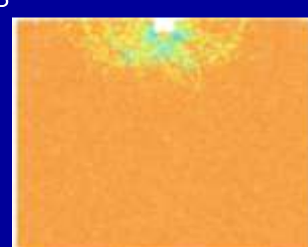

Rotations Color Bar for Rotations Figures (deg)

Shallow Foundation Results

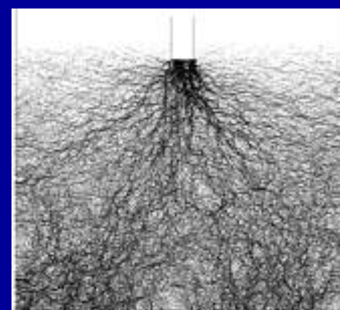

Shallow Foundation Force Chains at Baseline, Extended Height, and Extended Width Model Size (CW Respectively). Vertical Displacements are 0.20B for all cases shown.

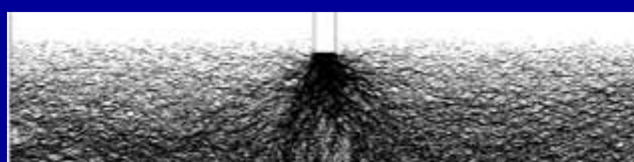

Deep Foundation Models

Deep Foundation:

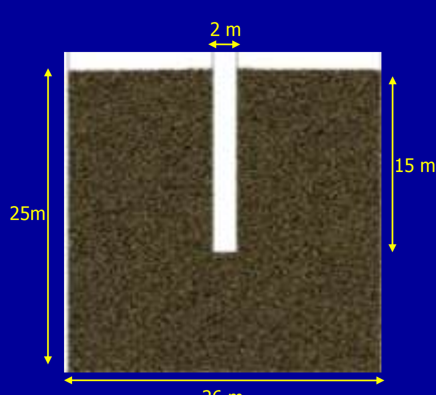

Deep Foundation Parametric Analysis

Parametric Case No.	Description	Model Dimensions (Height x Width)	Foundation Wall Friction
1	Low Friction	25 m x 26 m	μ = 0.155
2	Baseline	25 m x 26 m	μ = 0.31
3	High Friction	25 m x 26 m	μ = 0.46
4	Very High Friction	25 m x 26 m	μ = 0.62
5	Extended Width	36 m x 25 m	μ = 0.31
6	Extended Height	26 m x 35 m	μ = 0.31

Deep Foundation Models

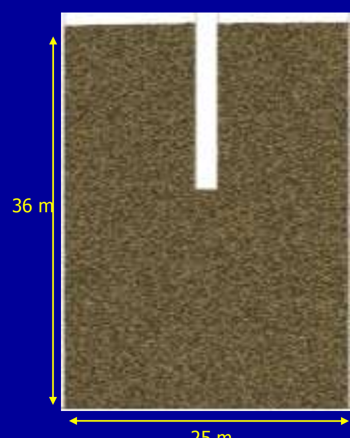

Deep Foundation Extended Height Assembly

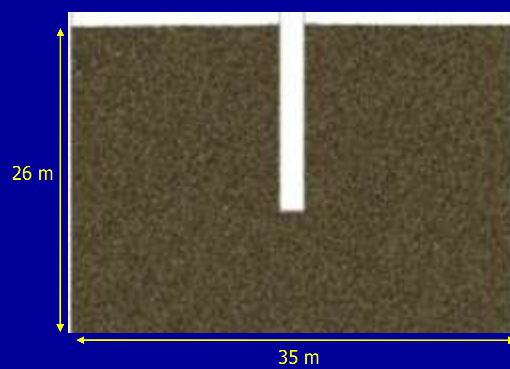

Deep Foundation Extended Width Assembly

Soil-Structure Interaction

Deep Foundation Results

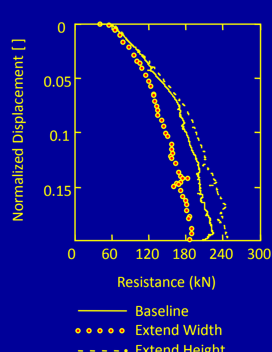

Deep Foundation Model Dimensions Total Resistance

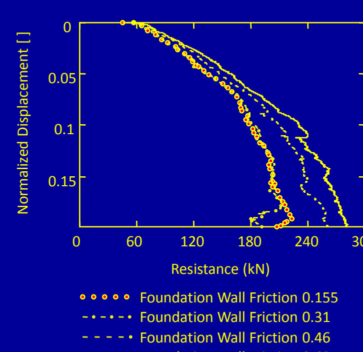

Deep Foundation Friction Total Resistance

Deep Foundation Results

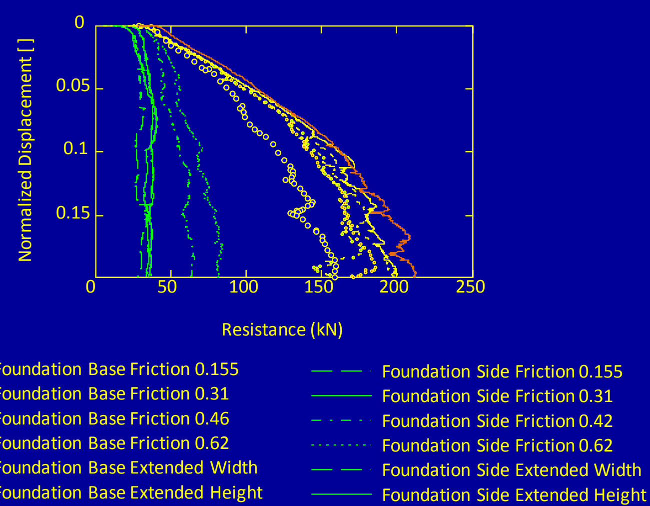

Deep Foundation Toe versus Side Resistance

Soil-Structure Interaction

Deep Foundation Results

δ = 0.00B

Deep Foundation Grain Rotations at 0.00B, Vertical Displacement

Rotations Color Bar for Rotations Figures (deg)

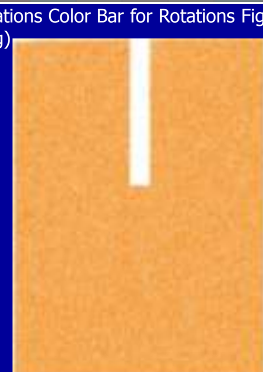

Soil-Structure Interaction

Deep Foundation Results

δ = 0.05B

Deep Foundation Grain Rotations
at 0.05B, Vertical Displacement

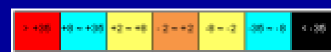

Rotations Color Bar for Rotations Figures
(deg)

Soil-Structure Interaction

Deep Foundation Results

δ = 0.10B

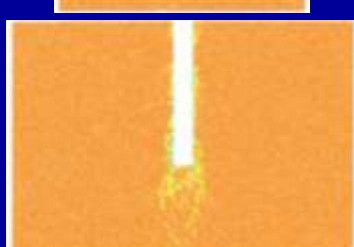

Deep Foundation Grain Rotations
at 0.10B, Vertical Displacement

Rotations Color Bar for Rotations Figures
(deg)

Deep Foundation Results

δ = 0.15B

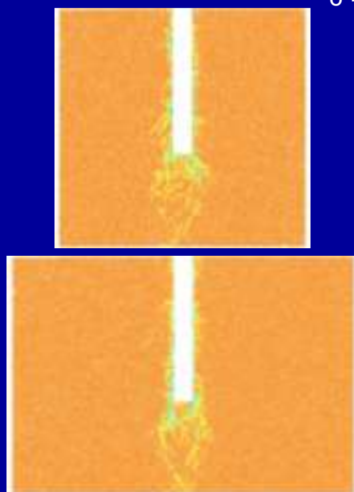

Deep Foundation Grain Rotations at 0.15B, Vertical Displacement

Rotations Color Bar for Rotations Figures (deg)

Soil-Structure Interaction

Deep Foundation Results

δ = 0.20B

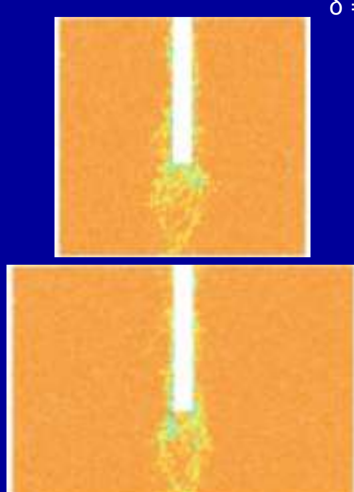

Deep Foundation Grain Rotations at 0.20B, Vertical Displacement

Rotations Color Bar for Rotations Figures (deg)

Deep Foundation Results

δ = 0.25B

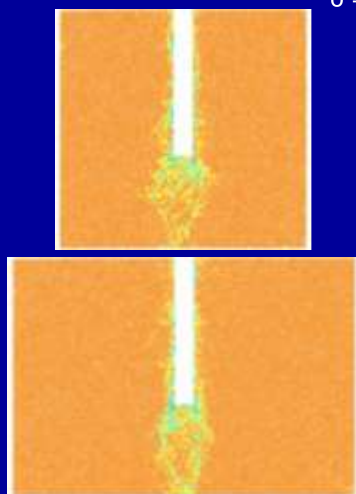

Deep Foundation Grain Rotations at 0.25B, Vertical Displacement

Rotations Color Bar for Rotations Figures (deg)

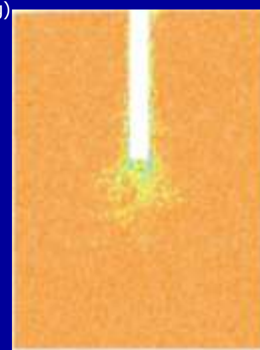

Laterally Loaded Pile Model

Laterally Loaded Pile:

- Pile Center of Mass
- 0.01 rad/s rotation
- 0.1B total rotation
- 1.8° total rotation

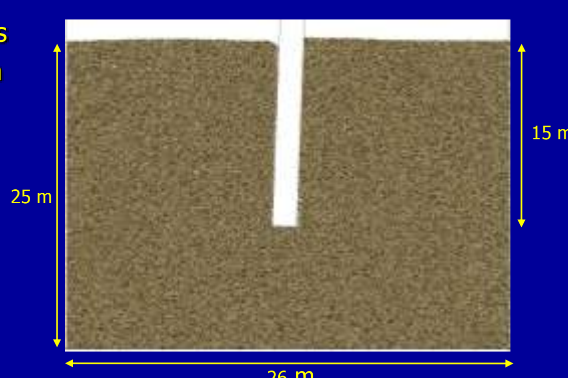

Shallow Foundation Model Dimensions Total Resistance

Laterally Loaded Pile Results

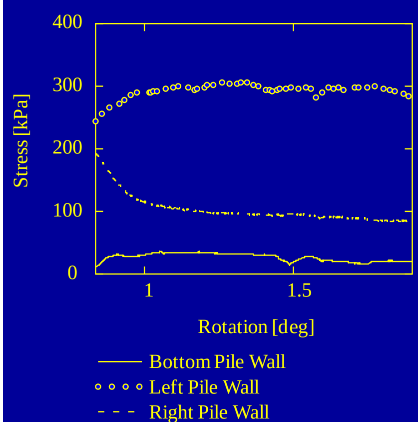

Deep Foundation Lateral Loading Lateral Stresses on Foundation Wall

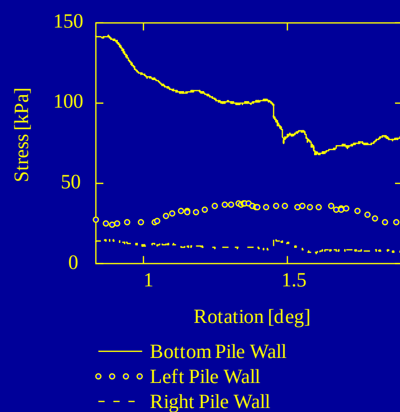

Deep Foundation Lateral Loading Vertical Stresses on Foundation Wall

Soil-Structure Interaction

Laterally Loaded Pile Results

$\delta = 0.00B$

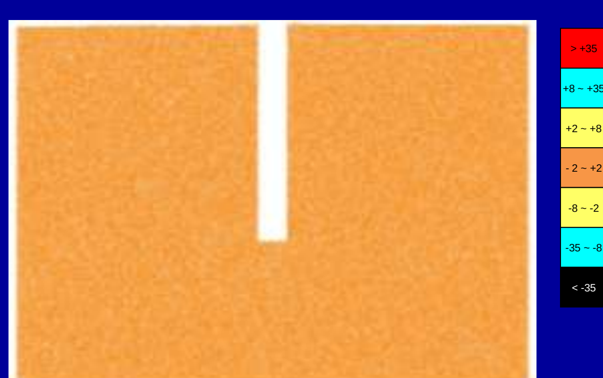

Deep Foundation Lateral Loading Grain Rotations at 0.00B Pile Rotation

Soil-Structure Interaction

Laterally Loaded Pile Results

δ = 0.05B

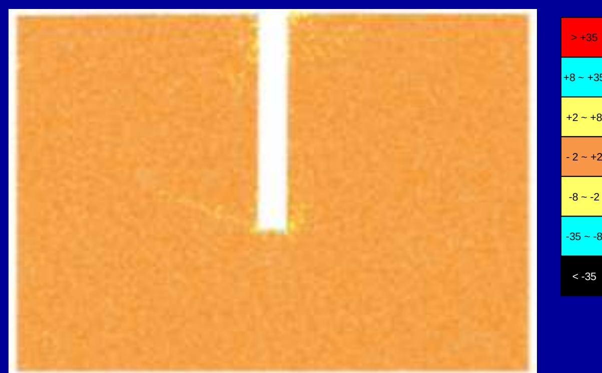

Deep Foundation Lateral Loading Grain Rotations at 0.05B Pile Rotation

Soil-Structure Interaction

Laterally Loaded Pile Results

δ = 0.10B

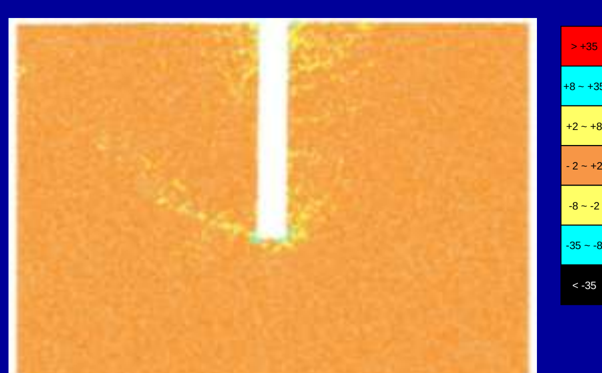

Deep Foundation Lateral Loading Grain Rotations at 0.10B Pile Rotation

Laterally Loaded Pile Results

δ = 0.15B

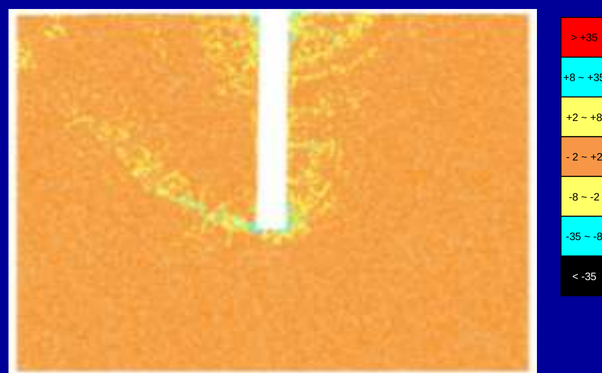

Deep Foundation Lateral Loading Grain Rotations at 0.15B Pile Rotation

Soil-Structure Interaction

Laterally Loaded Pile Results

δ = 0.20B

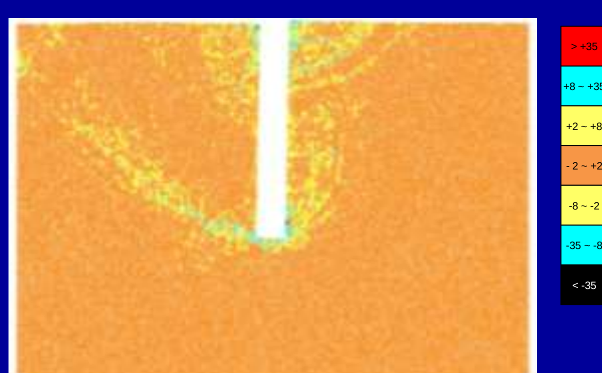

Deep Foundation Lateral Loading Grain Rotations at 0.20B Pile Rotation

Laterally Loaded Pile Results

δ = 0.25B

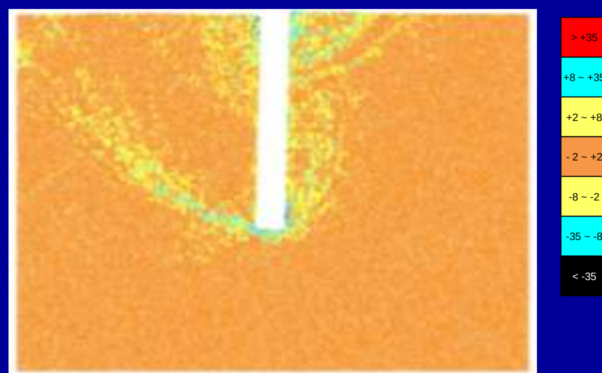

Deep Foundation Lateral Loading Grain Rotations at 0.25B Pile Rotation

Soil-Structure Interaction

Laterally Loaded Pile Results

δ = 0.30B

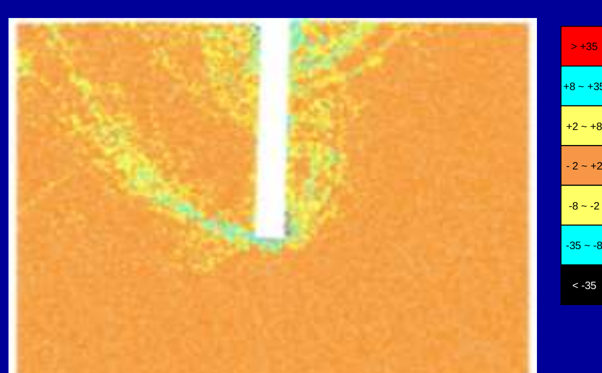

Deep Foundation Lateral Loading Grain Rotations at 0.30B Pile Rotation

Laterally Loaded Pile Results

δ = 0.35B

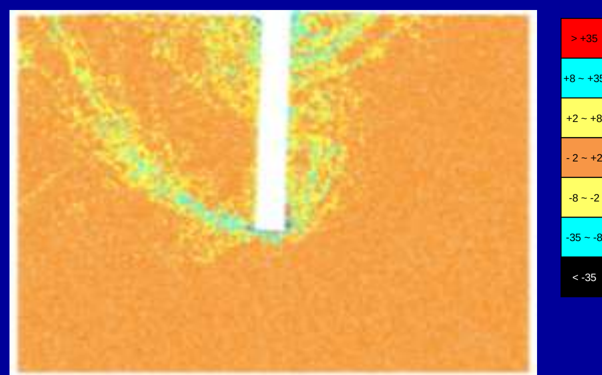

Deep Foundation Lateral Loading Grain Rotations at 0.35B Pile Rotation

Soil-Structure Interaction

Laterally Loaded Pile Results

δ = 0.40B

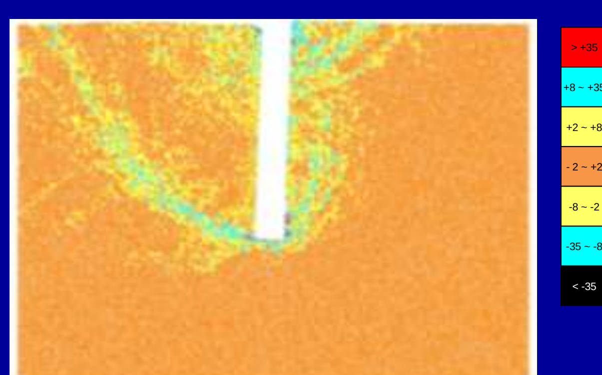

Deep Foundation Lateral Loading Grain Rotations at 0.40B Pile Rotation

Soil-Structure Interaction

Laterally Loaded Pile Results

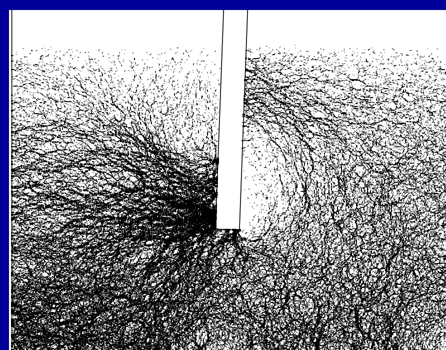

Deep Foundation Lateral Loading Force Chains at 0.1B Pile Rotation

Soil-Structure Interaction

Laterally Loaded Pile Results

Deep Foundation Lateral Loading Vertical Stress at 0.1B Pile Rotation (Units: Pa)

Deep Foundation Lateral Loading Lateral Stress at 0.1B Pile Rotation (Units: Pa)

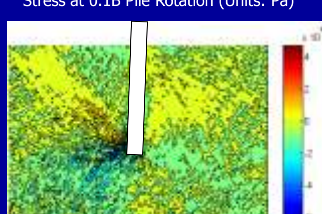

Deep Foundation Lateral Loading Shear Stress at 0.1B Pile Rotation (Units: Pa)

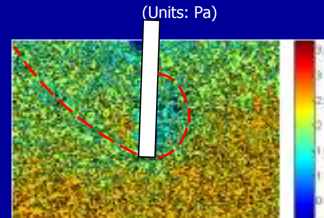

Deep Foundation Lateral Loading Coordination Number at 0.1B Pile Rotation

Rigid Retaining Walls

Rigid Retaining Wall:

- 30 m x 12 m (W x H)
- Models sizes same as for shallow foundations
- Lateral displacement of rigid wall

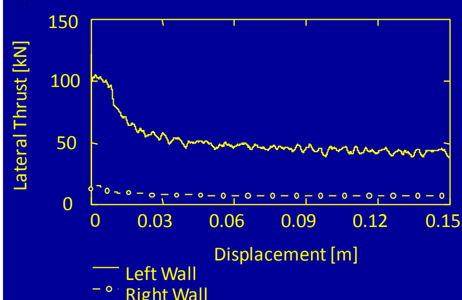

Rigid Retaining Wall Load-Displacement
Active Case

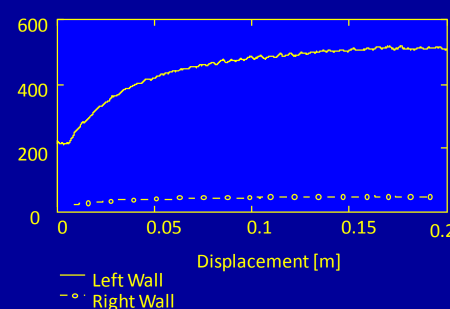

Rigid Retaining Wall Load-Displacement
Passive Case

Rigid Retaining Walls

δ = 0.00B

Rigid Retaining Wall Active Grain Rotations at 0.00B, Vertical Displacement

Rotations Color Bar for Rotations Figures (deg)

Rigid Retaining Walls

$\delta = 0.05B$

Rigid Retaining Wall Active Grain Rotations at 0.05B, Vertical Displacement

Rotations Color Bar for Rotations Figures (deg)

Rigid Retaining Walls

$\delta = 0.10B$

Rigid Retaining Wall Active Grain Rotations at 0.10B, Vertical Displacement

Rotations Color Bar for Rotations Figures (deg)

Rigid Retaining Walls

δ = 0.15B

Rigid Retaining Wall Active Grain Rotations at 0.15B, Vertical Displacement

Rotations Color Bar for Rotations Figures (deg)

Rigid Retaining Walls

δ = 0.20B

Rigid Retaining Wall Active Grain Rotations at 0.20B, Vertical Displacement

Rotations Color Bar for Rotations Figures (deg)

Rigid Retaining Walls

δ = 0.05B

Rigid Retaining Wall Passive Grain Rotations at 0.05B, Vertical Displacement

Rotations Color Bar for Rotations Figures (deg)

Rigid Retaining Walls

δ = 0.10B

Rigid Retaining Wall Passive Grain Rotations at 0.10B, Vertical Displacement

Rotations Color Bar for Rotations Figures (deg)

Rigid Retaining Walls

δ = 0.15B

Rigid Retaining Wall Passive Grain Rotations at 0.15B, Vertical Displacement

Rotations Color Bar for Rotations Figures (deg)

Rigid Retaining Walls

δ = 0.20B

Rigid Retaining Wall Passive Grain Rotations at 0.20B, Vertical Displacement

Rotations Color Bar for Rotations Figures (deg)

Rigid Retaining Walls

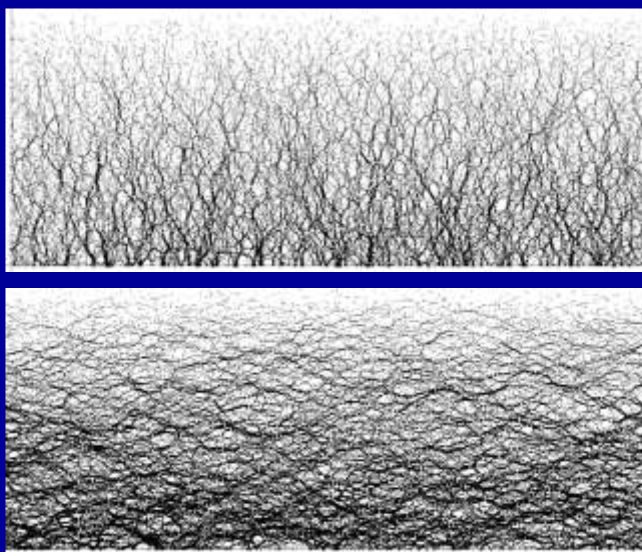

Rigid retaining wall active force chains (top) and passive force chains (bottom). Retaining wall lateral displacement is 0.10 m.

Shallow Foundation Load-Displacement

Akbas & Kulhawy (2009a) Hyperbolic Method:

$$\frac{Q}{Q_{L2}} = \left[\frac{\rho/B}{a(\rho/B)+b}\right]$$

Hyperbolic fit equation. Parameters *a* and *b* are 0.70 and 1.77 respectively for residual soils and 0.69 and 1.68 respectively for cemented soils

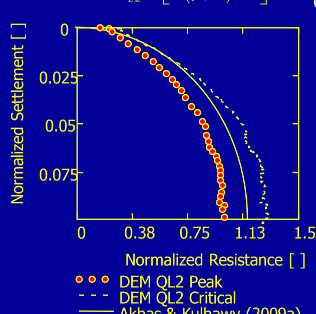

Shallow Foundation Normalized DEM & Hyperbolic Fit

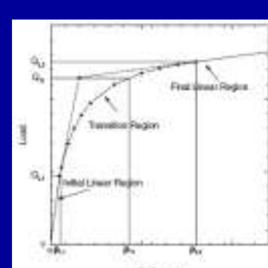

Definition of Q_{L2} (After Akbas and Kulhawy 2009a)

Shallow Foundation Bearing Capacity

<u>Shallow Foundation</u>:

Bearing Capacity (effective stress analysis):

$$q_{ult} = \gamma D_f (N_q - 1) d_q + 0.5 \gamma B N_\gamma d_\gamma$$

Where: $N_q = e^{\pi \tan\phi'} \tan\left(\frac{\pi}{4} + \frac{\phi'}{2}\right)^2$

Ueno et al. (1998):

$$N_\gamma = 0.477 e^{6.52\phi'}$$

Allowable Load:

$$q_a = \left(\frac{q_{ult}}{F.S.} + \gamma D_f\right)$$

Shallow Foundation Bearing Capacity

<u>Shallow Foundation Bearing Capacity</u>:

- At Φ'_p
  - Ultimate Load = 246.6 kN
  - Allow FS 1.5 = 168.9 kN
  - Allow FS 3.0 = 86.8 kN

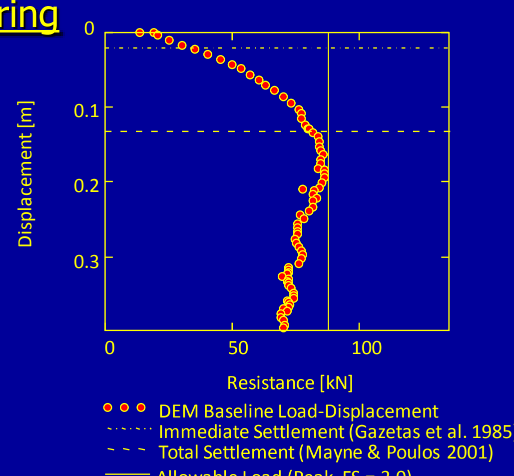

Soil-Structure Interaction

Shallow Foundation Failure Surfaces

$r(\theta) = r_0 e^{\theta \tan(\phi')}$ $\theta = (\pi/4) \pm (\phi'/2)$

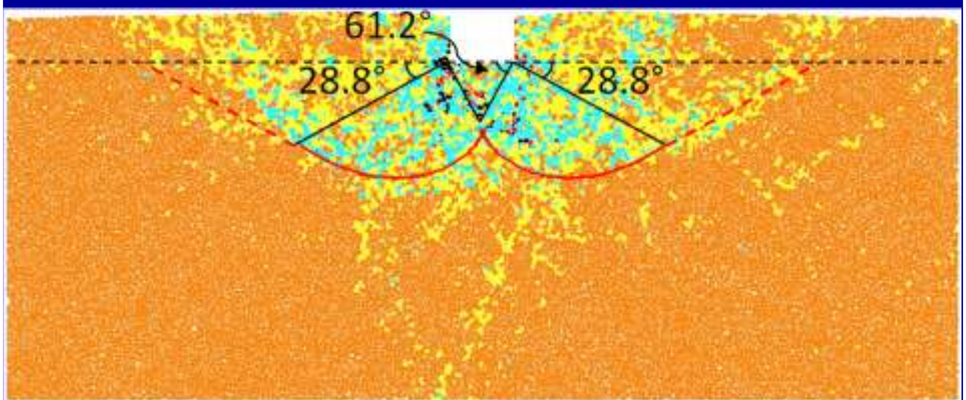

Grain Rotations Shallow Foundation Baseline at 0.20B Vertical Displacement (computed at ϕ'_{peak})

Soil-Structure Interaction

Pile Lateral Load-Deflection

- Analytical Solution (Matlock and Reese, 1962)
- m_h is related to the subgrade modulus for the soil response along the pile

$$\rho_L = 2.43 \frac{P_x}{m_h} \left(\frac{l_c}{4}\right)^{-2} + 1.62 \frac{M}{m_h} \left(\frac{l_c}{4}\right)^{-3}$$

$$\theta = 1.62 \frac{P_x}{m_h} \left(\frac{l_c}{4}\right)^{-3} + 1.73 \frac{M}{m_h} \left(\frac{l_c}{4}\right)^{-4}$$

$$l_c = 4 \left(\frac{E_p I_p}{m_h}\right)^{1/5}$$

- $M = 0$; P_x is reaction at ground surface from compressive forces acting on the pile in the subgrade
- Lateral deflection at ground surface to be approximately 0.065 m and rotation of the pile walls to be approximately 0.318°

Soil-Structure Interaction

Pile Lateral Load-Deflection

Laterally Loaded Pile:

- DEM Results (AutoCAD measurements)

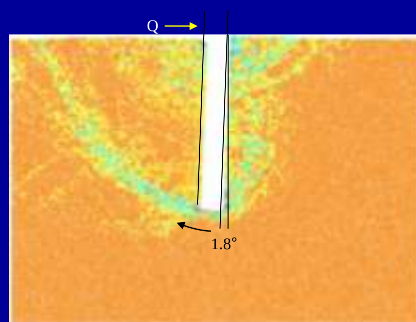

Deep Foundation Laterally Loaded Pile Rotation Quantification

Soil-Structure Interaction

Pile Lateral Load-Deflection

Laterally Loaded Pile:

- DEM Results (AutoCAD measurements)
- Set to 0.25^{0}, determine lateral displacement along ground surface

Deep Foundation Laterally Loaded Pile Rotation at 0.25 (deg)

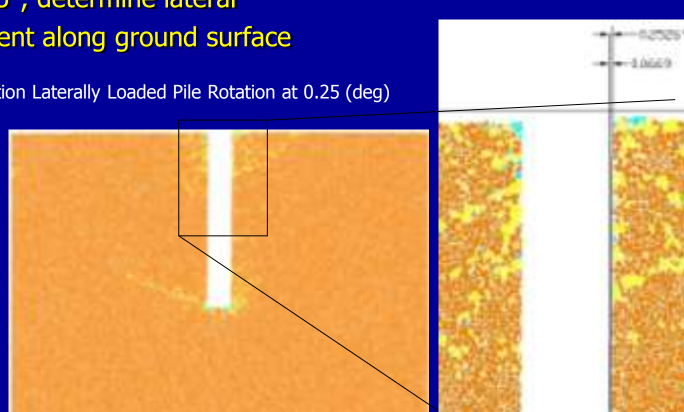

Rigid Wall Force Mobilization

- Deflections required for full mobilization of active or passive thrust (after Salgado 2008)

Soil Type	Active State (δ_h/H_0)	Passive State (δ_h/H_0)
Dense Sand	0.001	0.020
Loose Sand	0.004	0.060
Stiff Clay	0.010	0.020
Soft Clay	0.020	0.040

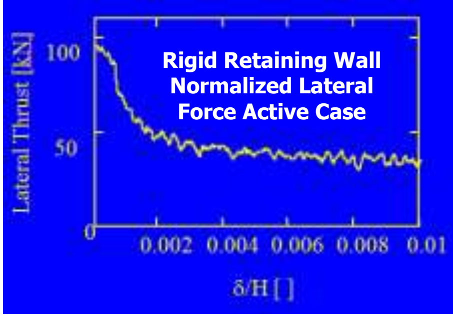

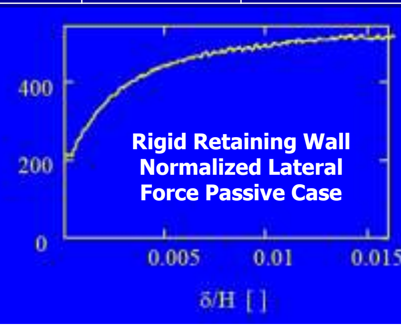

Rigid Wall Earth Stress Coefficients

Active Case Analytical Versus DEM Results (at ϕ'_{cs})

Description	Formulation (Theoretical)	Theoretical Value (A)	DEM Simulation Value (B)
Orientation [deg]	$\theta_a = \frac{\pi}{4} + \frac{\phi'}{2}$	58.3	60 – 65 (rot figs)
Normalized Lateral Wall Deflection [ ]	$\frac{\delta_a}{H_0}$	0.001	0.001 - 0.004
Earth Pressure Coefficient [ ]	$K_a = \frac{1 - sin(\phi')}{1 + sin(\phi')}$	0.38	0.32
Lateral Thrust [kN]	$P_a = \int_0^{H_0} K_a \gamma' z dz$	48.4	37.9

Rigid Wall Earth Stress Coefficients

Passive Case Analytical Versus DEM Results (at ϕ'_{cs})

Description	Formulation (Theoretical)	Theoretical Value (A)	DEM Simulation Value (B)
Orientation [deg]	$\theta_a = \frac{\pi}{4} + \frac{\phi'}{2}$	31.7	30 – 36 (rot figs)
Normalized Lateral Wall Deflection [ ]	$\frac{\delta_a}{H_0}$	0.020	0.004 - 0.015
Earth Pressure Coefficient [ ]	$K_a = \frac{1-sin(\phi')}{1+sin(\phi')}$	2.62	3.16
Lateral Thrust [kN]	$P_a = \int_0^{H_0} K_a \gamma' z dz$	533.4	507.9

Overview

- Soil micromechanics
- Discrete element method (DEM)
- Integrated Numerical-Experimental Study
- DEM Simulations: Effects of Geometry
- Soil-Structure Interaction (SSI)
- Thermal Conductivity
- Summary and Conclusions

Heat in Soils

- Historically ignored or considered insignificant in geotechnical engineering
- 98% of Earth's volume has T>1000°C
- Heat flux in oceans and climate change are observable manifestations of geothermal processes
- Important in alternative energy and waste isolation applications
- Coupled thermo-hydro-mechanical response incredibly difficult to model (fully-coupled multiphysics simulations)

Thermal Properties of Soils

- Specific Heat: heat required to raise the temperature of a unit mass of material by 1 K (bulk property, scalar, $J \cdot kg^{-1}K^{-1}$)
- Thermal Conductivity: heat flow per unit temperature gradient (transport property, scalar, $W \cdot m^{-1}K^{-1}$)
- Thermal Diffusivity: governs rate of spread of temperature disturbances (bulk property, scalar, m^2s^{-1})
- Coefficient of Thermal Expansion: measures fractional change in size per unit temperature change (bulk property, scalar, K^{-1})

$$Q = mc\Delta T$$

$$\dot{q} = -\lambda \nabla T$$

$$D = \frac{\lambda}{c\rho}$$

$$\frac{dL}{dT} = \alpha_L L$$

Thermal Properties of Soils

	Specific Heat [J·kg^{-1}K^{-1}]	Volumetric Heat Capacity [J·m^{-3}K^{-1}]	Thermal Conductivity [W·m^{-1}K^{-1}]	Thermal Diffusivity [m^{2}s^{-1}]	Coefficient of Volume Thermal Expansion [K^{-1}]
Solid	750	2×10^6	8	1×10^{-6}	15×10^{-6}
Water	4184	4×10^6	0.56	9×10^{-8}	207×10^{-6}
Air	1000	1×10^3	0.024	4×10^{-9}	$1/T_0$

Additional Notes:
1. Values given for solids are representative of soil minerals.
2. Volumetric heat capacity is specific heat multiplied by mass density.
3. Can you prove that $\alpha_V=1/T_0$ for air?

Thermal Conductivity of the Matrix

- Consider a dry (two-phase) soil. We can approximate thermal conductivity of the matrix using semi-empirical or analytical approaches.
- Semi-empirical:

Equation	Notes	Reference
$\lambda = \frac{0.1781}{n+0.056} - 0.1447$	λ in W/m·K G_s=2.7	Johansen, 1975, lower estimate
$\lambda = 0.039 n^{-2.2}$	λ in W/m·K	Johansen, 1975, upper estimate
$\lambda = 0.025 + 0.238\rho_d - 0.193\rho_d^2 + 0.114\rho_d^3$	λ in W/m·K ρ in g/cm^3	Gavriliev, 2004

- Analytical: next slide

(after Yun and Santamarina, 2008)

Thermal Conductivity of the Matrix

Model	Equation	Reference
Series	$\lambda_{eff} = \left(\sum_i \frac{n_i}{\lambda_i}\right)^{-1}$	DeVera, and Strieder, 1977
Parallel	$\lambda_{eff} = \sum_i n_i \lambda_i$	DeVera, and Strieder, 1977
Geometric Mean	$\lambda_{eff} = \prod_i \lambda_i^{n_i}$	Sass, et al., 1971
Hashin and Shtrikman Boundary	$\lambda_{eff} = \lambda_1 \left[1 + \frac{3n_2(\lambda_2 - \lambda_1)}{3\lambda_1 + n_1(\lambda_2 - \lambda_1)}\right]$	Hashin and Shtrikman, 1962
Self-Consistent	$\lambda_{eff} = \frac{1}{3}\left[\frac{1-n}{2\lambda_{eff} + \lambda_m} + \frac{n}{2\lambda_{eff} + \lambda_a}\right]^{-1}$	Hill, 1965

NOTE: For HSL, 1=solid, 2=pore; for HSU, 1=pore, 2=solid.

(after Yun and Santamarina, 2008)

Thermal Conduction

Heat Transport in Soils

- Five primary mechanisms
  - Conduction (dominates in solid phase)
  - Convection (dominates in liquid phase)
  - Radiation (no material medium required)
  - Vaporization/condensation (partially saturated soils)
  - Ion exchange (flow of water through clays)
- Big players: conduction, convection

Conduction

- Heat is transferred by molecular excitation of stationary materials
- Governed by Fourier's Law
  - Differential form: $\dot{q} = -\lambda \nabla T$
  - Integral form: $\dfrac{\partial Q}{\partial t} = -\lambda \oint_S \vec{\nabla} T \cdot d\vec{A}$

(after McCartney, 2009)

Convection

- Transfer of heat between two thermodynamic systems moving relative to one another
- Newton's Law of Cooling
  - For water: $\dot{q}_w = c_w \rho_w v_w \left(T - T'\right)$

The Heat Equation

- Assuming conduction only, we can combine Fourier's Law with the continuity equation to get the Heat Equation
  - Fourier's Law: $\dot{q} = -\lambda \nabla T$
  - Continuity: $-\rho c \frac{\partial T}{\partial t} = \nabla \dot{q}$
  - Combining: $-\rho c \frac{\partial T}{\partial t} = \nabla\left(-\lambda \nabla T\right)$
  - Which gives us: $\frac{\partial T}{\partial t} = \frac{\lambda}{\rho c} \nabla^2 T$

Heat Conduction in the Ground

- One-dimensional heat conduction equation is:

$$\frac{\partial T\left(x,t\right)}{\partial t} = \frac{\lambda}{c\rho} \frac{\partial^2 T\left(x,t\right)}{\partial x^2}$$

- During the year, the surface temperature is a sinusoidal function:

$$T(0,t) = T_0 \sin\left(\omega t\right) + \overline{T}$$

- The analytical solution is:

$$T\left(x,t\right) = T_0 \exp\left[-\sqrt{\frac{\omega \rho c}{2\lambda}} x\right] \sin\left[\omega t - \sqrt{\frac{\omega \rho c}{2\lambda}} x\right] + \overline{T}$$

(after Rongère, 2009)

Ground Temperature

- Ground temperature remains constant around the year for a depth greater than 10 m.
- Ground characteristics:
  - $T_0 = 20°C$
  - $\omega = 2.10^{-7}\ s^{-1}$
  - $\rho = 2{,}300\ kg \cdot m^{-3}$
  - $C = 900\ J \cdot kg^{-1} \cdot K^{-1}$
  - $k = 1.5\ W \cdot m^{-1} \cdot K^{-1}$

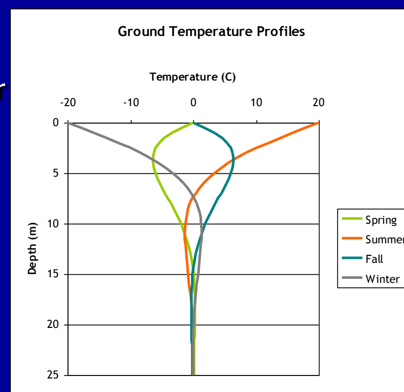

(after Rongère, 2009)

Thermal Conductivity: Existing Models

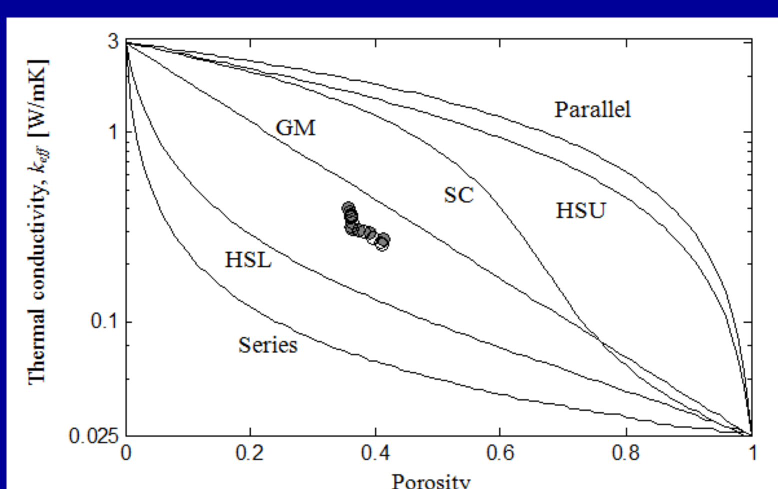

Thermal Conductivity: Discrete Models

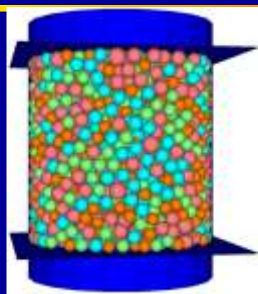

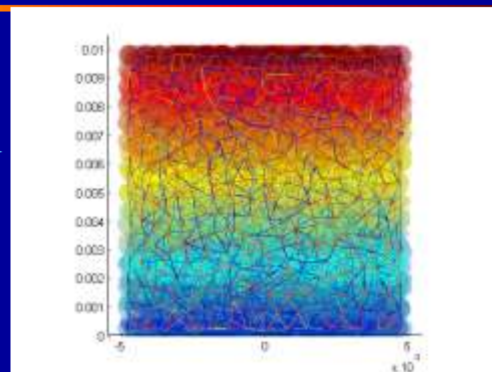

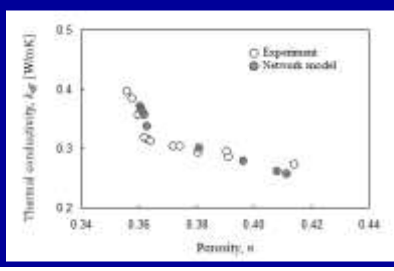

Yun, T.S. and T.M. Evans. (2010). "Three-dimensional random network model for thermal conductivity in particulate materials." *Computers and Geotechnics*, in press.

Summary and Conclusions

- Many (all?) macroscale behaviors are driven by microscale processes
- Enhanced understanding of soil micromechanics can lead to better understanding of design-scale soil behavior
- Discrete simulations can be used for micromechanical studies or applied to a variety of design problems
- Well-calibrated discrete simulations can reasonably predict soil behavior across multiple scales